



Figure 20. Nodule SCB 383-3: olivine=Fo-76.4; average grain size=1-3 mm; iridescent grain surfaces; friable. Note that lherzolite has a high percentage of dark (CPX, spinel) minerals.



Figure 21. Nodule SCB 383-4: olivine=Fo-79.6; average grain size=1 mm; no iridescent grain surfaces; not friable. Note thickness of veins relative to lherzolite rock.



Figure 22. Nodule SCB 383-6: olivine=Fo-76.7; average grain size=1-3 mm, with some large (5 mm) olivine grains; iridescent grain surfaces; friable. Note cross-cutting vein (arrow) connecting two parallel veins.

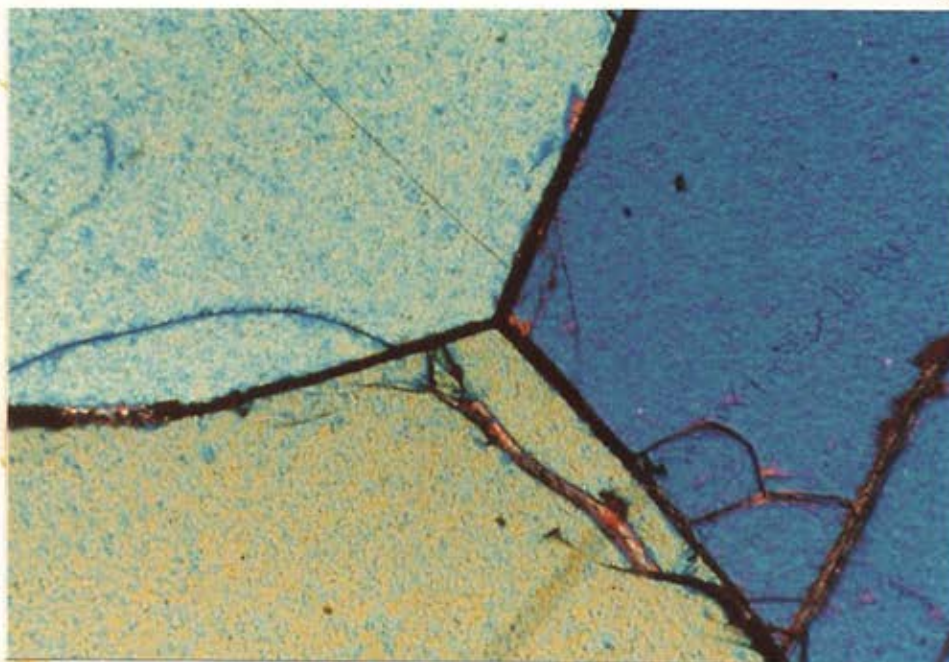


Figure 23. Near- $120^{\circ}$  intersections between three olivine grains. XPL, 1.0 x 0.71 mm.

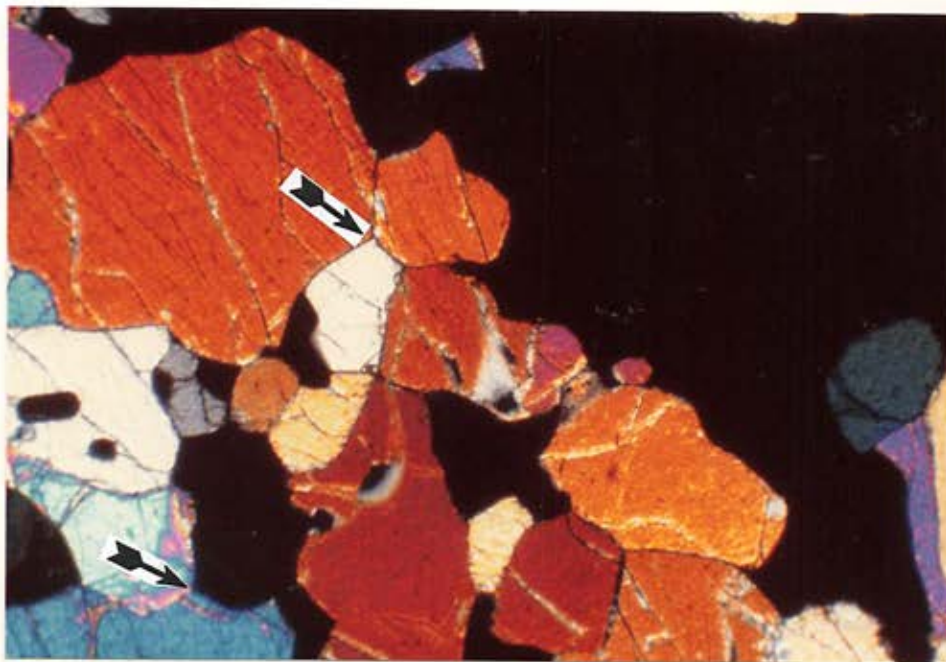


Figure 24. CPXite/lherzolite boundary with near- $120^{\circ}$  grain intersections (arrows). XPL, 2.8 x 2.0 mm.

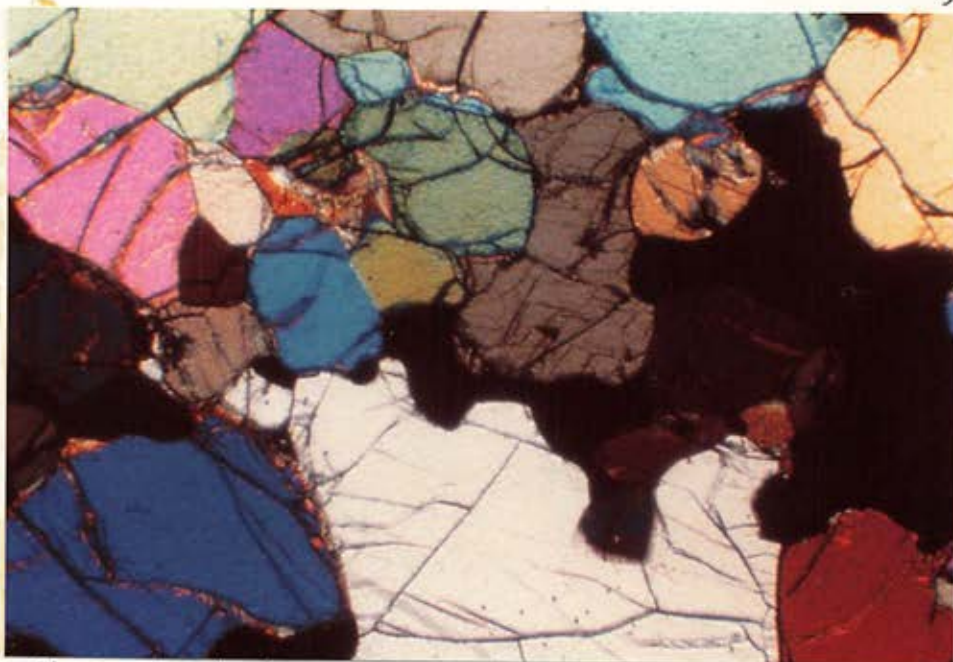
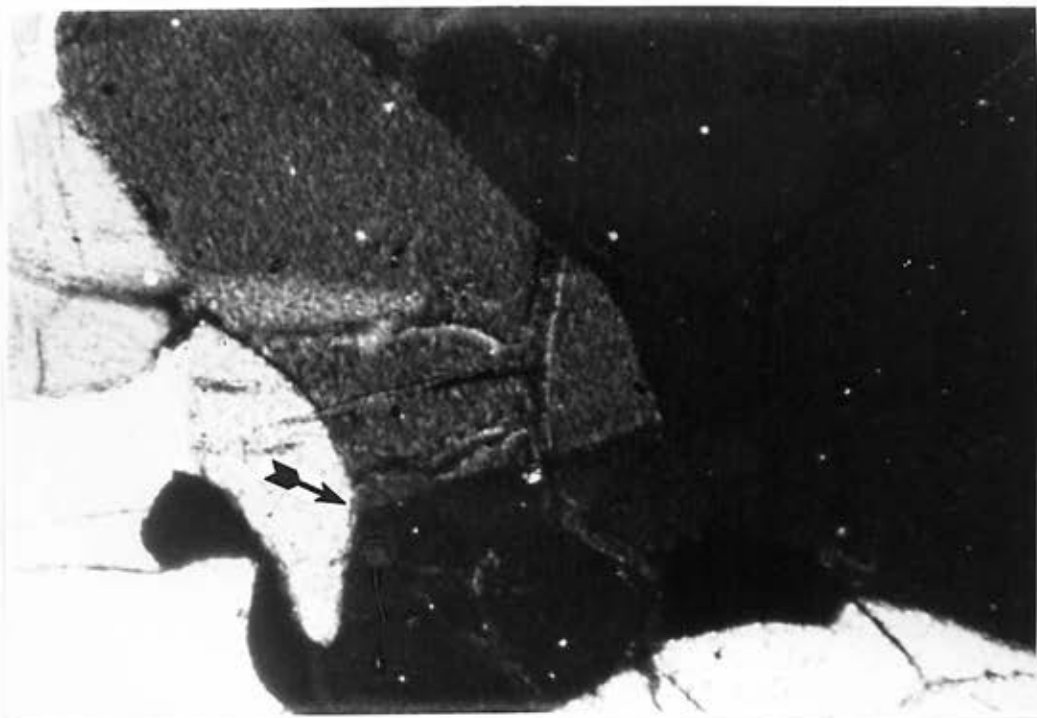


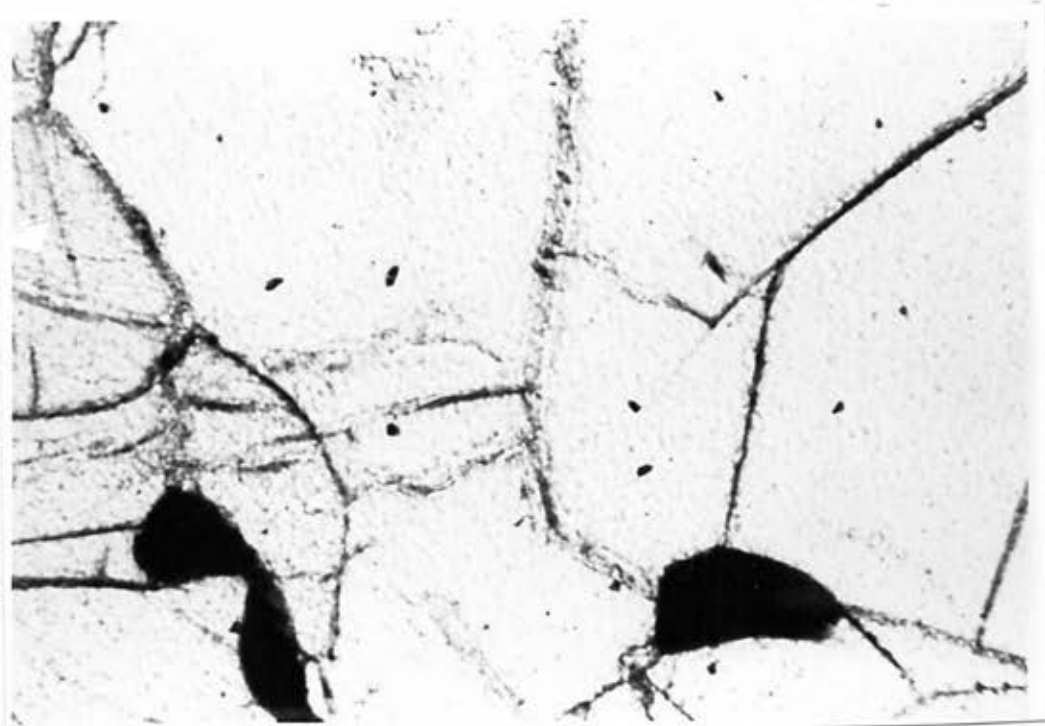
Figure 25. Characteristic texture in nodules of this study. Note mixture of near- $120^\circ$  intersections and non-angular grain interfaces and the variation in grain sizes. XPL, 2.8 x 2.0 mm.

Figure 26. (Next page) Kinked olivine apparently recrystallizing to smaller grains with a near- $120^\circ$  intersection (arrow). Both pictures are of the same area and are 1.0 x 0.71 mm field of view. 26a, XPL; 26b PPL. Note that extinction defined bands are not seen in PPL.

94a



26a



26b

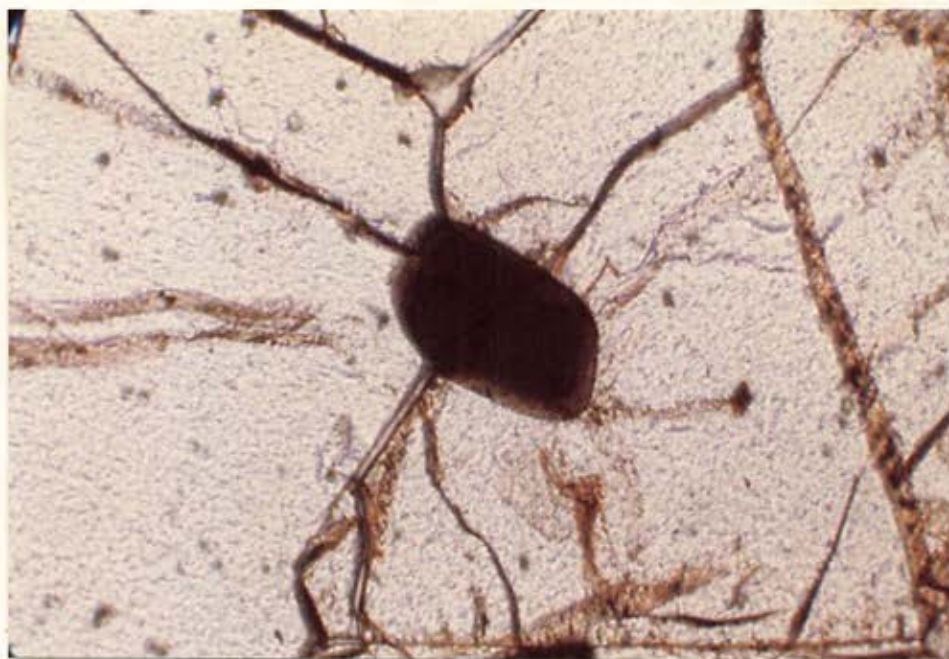


Figure 27. Cracks radiating from included spinel. PPL, 1.0 x 0.71 mm



Figure 28. Spinel types: holly leaf (H), grain boundary (G), included (I). PPL, 2.8 x 2.0 mm.

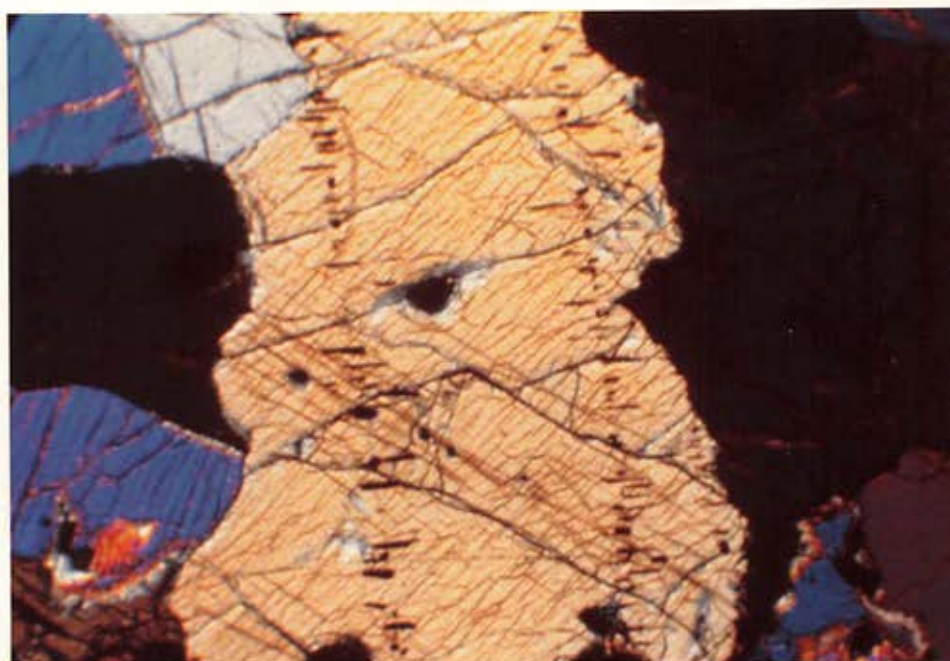


Figure 29. CPX with exsolved spinels. XPL, 2.8 x 2.0 mm.

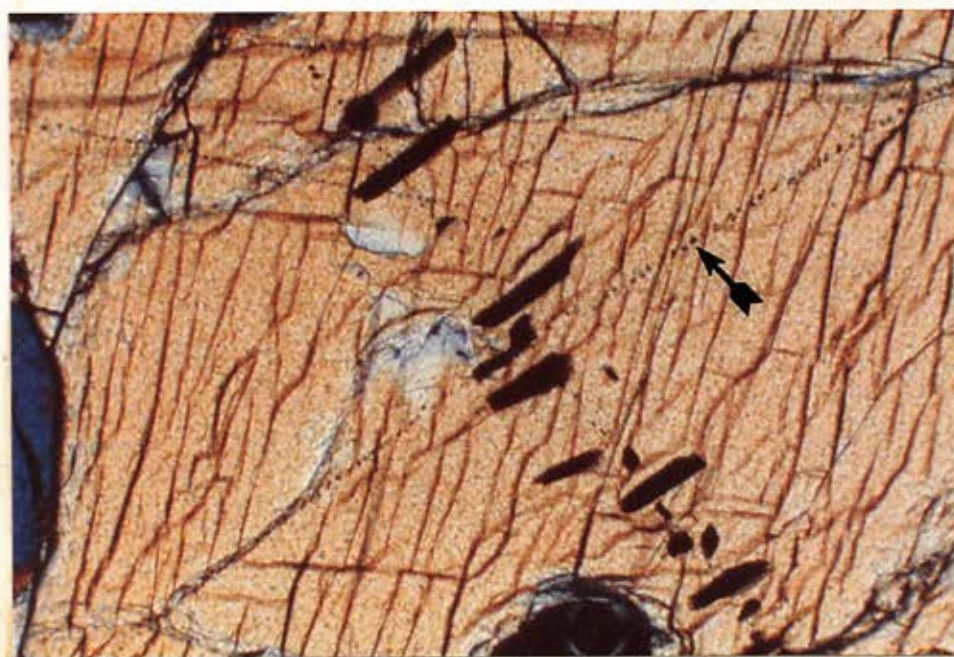


Figure 30. Close-up of Figure 29. Note trail of fluid inclusions (arrow) and numerous cracks in CPX. XPL, 1.0 x 0.71 mm.

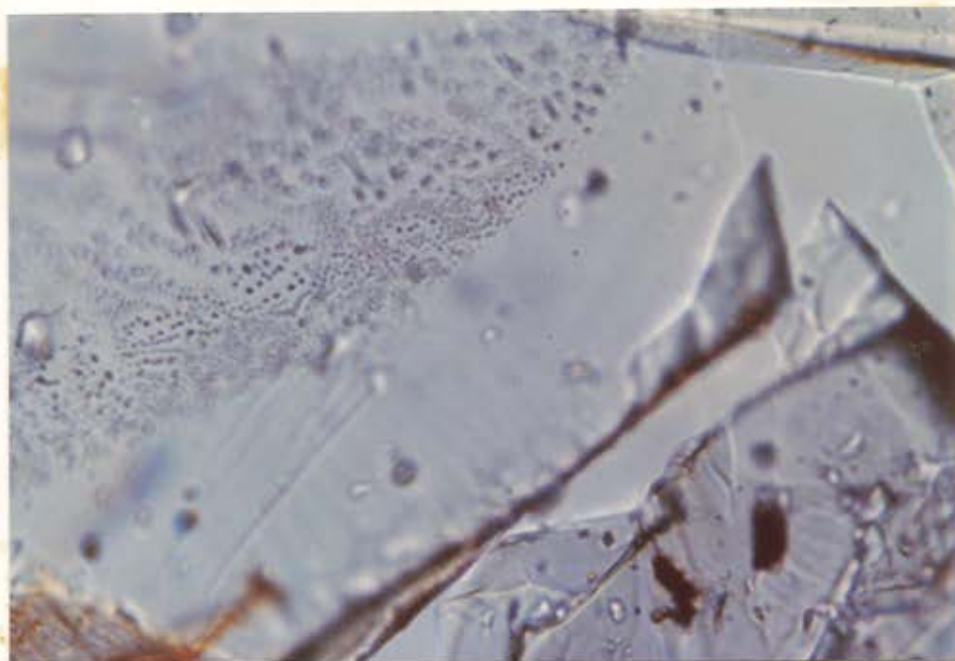


Figure 31. Group II olivine, grain mount in oil  $n=1.68$ . Note numerous fluid inclusions. PPL, 210 x 150 microns.

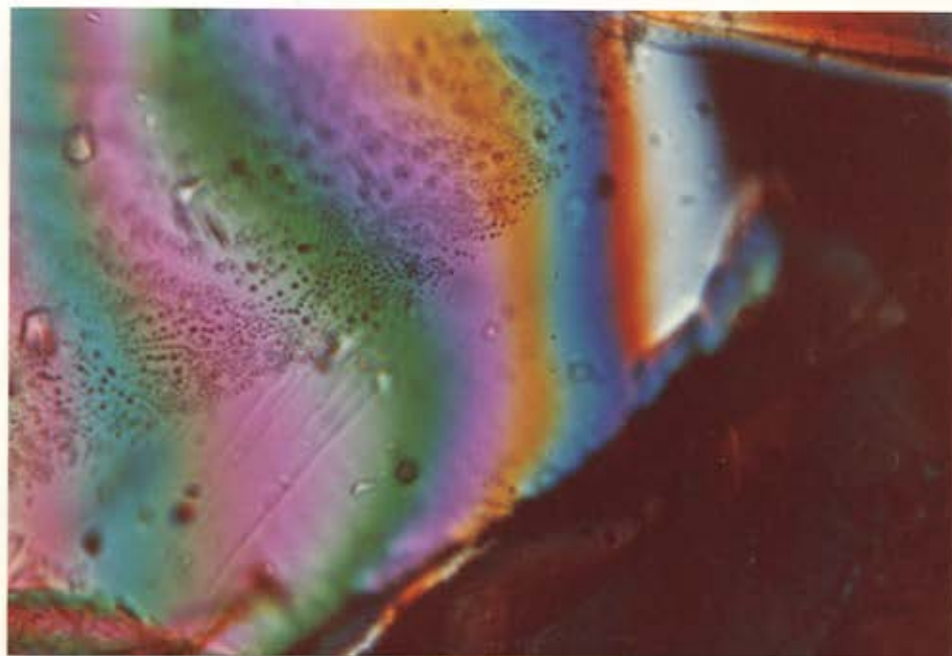


Figure 32. Same photo as Figure 31, but XPL. Note that grain is optically continuous (interference color bands). 210 x 150 microns.



Figure 33. Spongy grain borders (arrows), indicating incipient partial melting. XPL, 2.8 x 2.0 mm.

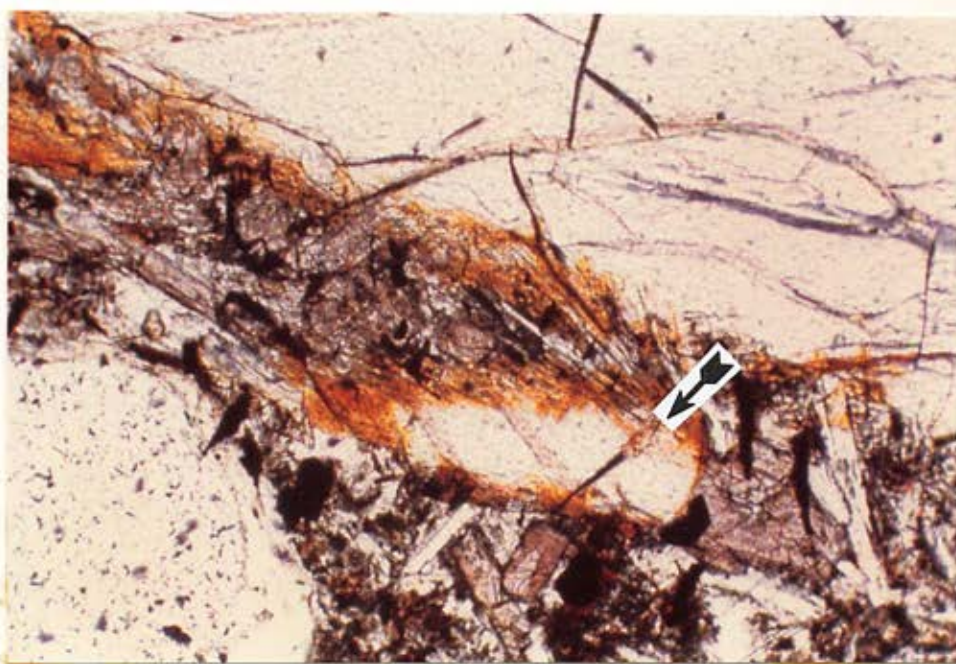


Figure 34. Partial melt channel. Note pyroxene "xenocryst" (arrow) in channel. PPL, 1.0 x 0.71 mm.

Figure 35. Cation distribution in Group II composite nodule minerals (this study).  $\bar{x}$  = mean values from microprobe data, s = standard deviation of data. Na value is high because of microprobe was not specifically set for Na analysis during this work.

## DATA

Clinopyroxene

Cation:	Na	Mg	Al	Ca	Si	$\Sigma$ Fe
$\bar{x}$ :	1.04	13.42	7.98	20.33	48.29	6.54
s:	0.10	0.18	0.25	0.36	0.41	0.20

Olivine

Cation:	Mg	Si	$\Sigma$ Fe
$\bar{x}$ :	40.05	38.42	21.36
s:	0.66	0.62	0.47

Spinel

Cation:	Mg	Al	Ti	Cr	Fe <sup>2+</sup>	Fe <sup>3+</sup>
$\bar{x}$ :	17.16	59.93	0.41	1.26	15.12	5.61
s:	0.35	1.10	0.05	0.64	0.58	0.74

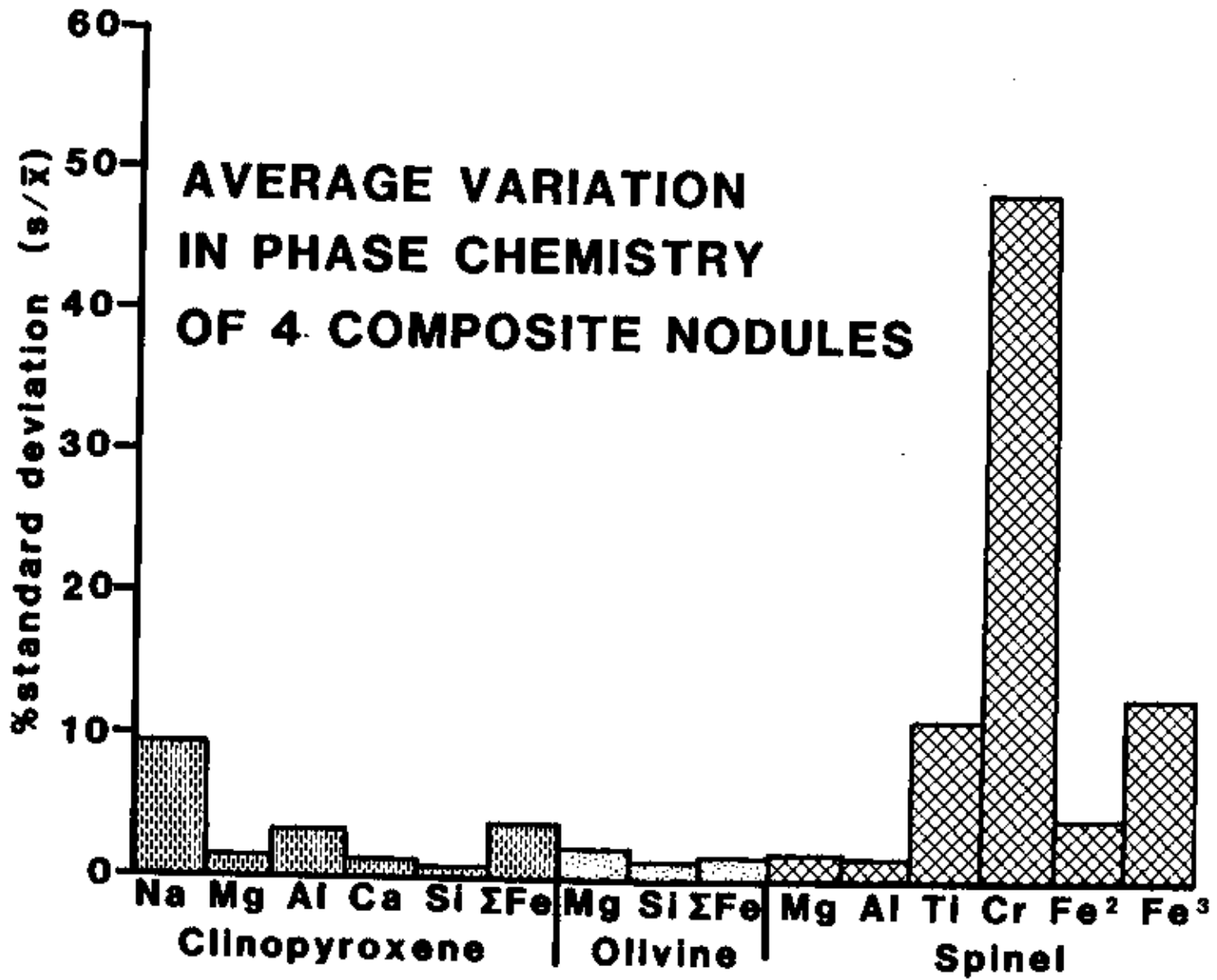
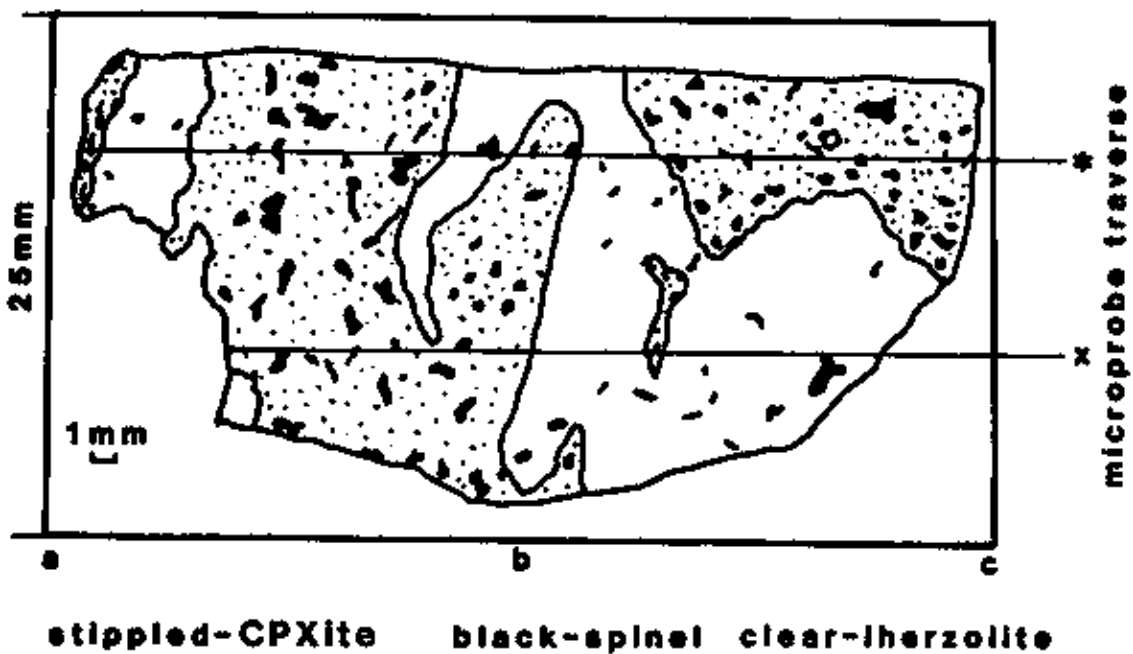


Figure 36.  $\text{Cr}_2\text{O}_3$  content of spinels,  
thin section SCB 383-1-1. Lherzolite area higher  
than CPXite. x represents bottom traverse, \* top  
traverse.

## THIN SECTION 1-1



## Cr Content of Spinels

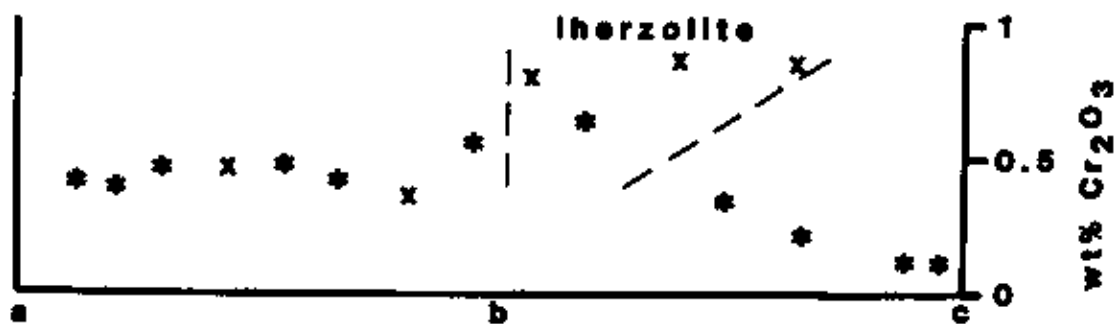
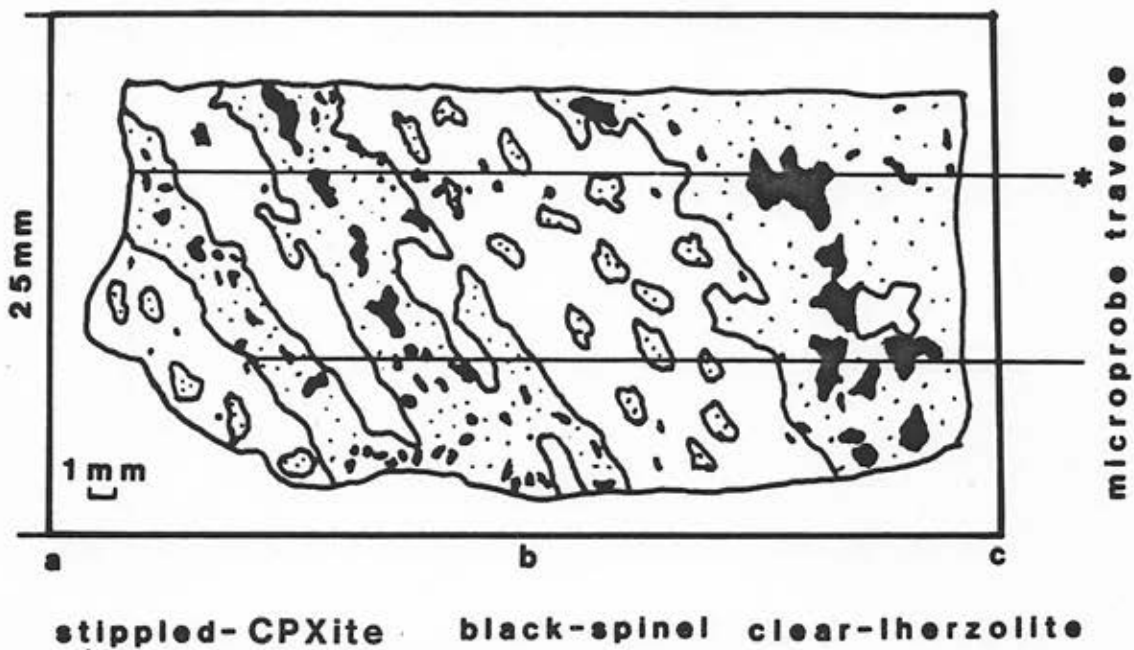


Figure 37.  $\text{Cr}_2\text{O}_3$  content of spinels,  
thin section SCB 383-2-2. Holly leaf spinels show  
lower levels than other spinel types. Only one  
traverse made (\*).

## THIN SECTION 2-2



## Cr Content of Spinels

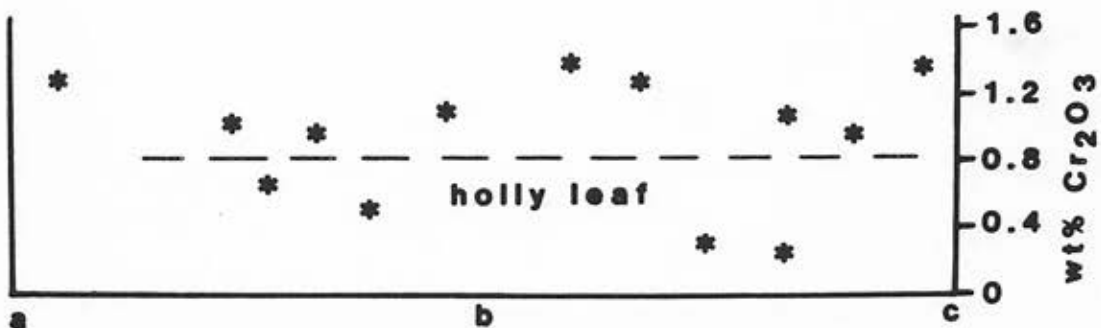
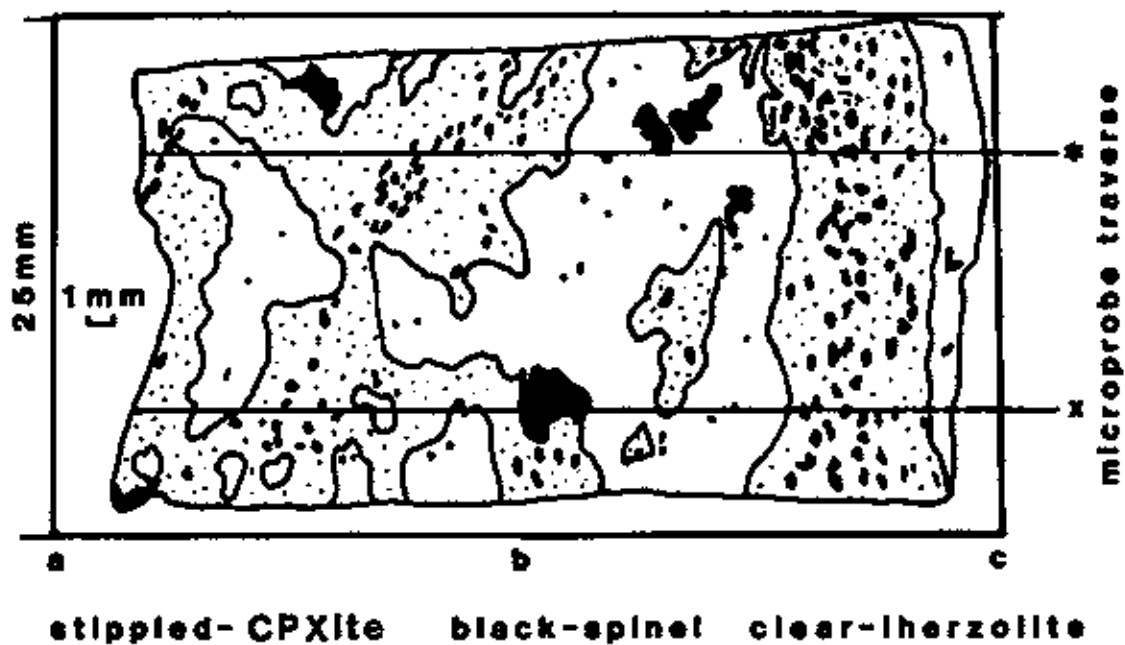
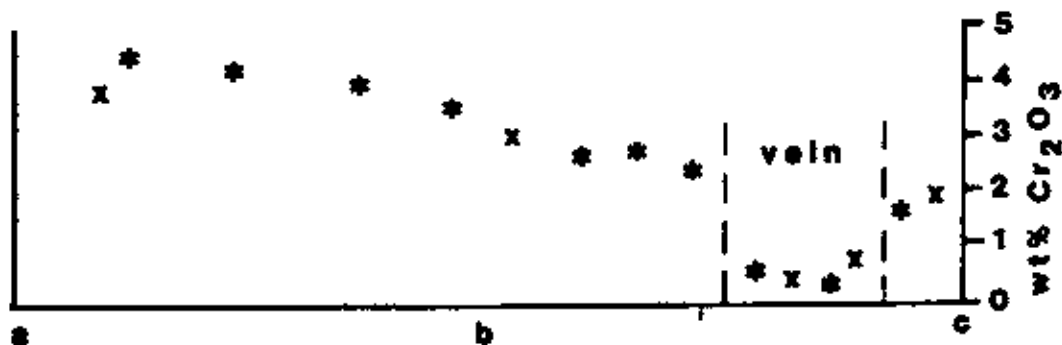


Figure 38.  $\text{Cr}_2\text{O}_3$  content of spinels,  
thin section SCB 393-3-1. Vein at right shows  
lower levels than all lherzolite, but note  
constant increase across lherzolite and CPXite  
areas to the left. x represents bottom traverse, \*  
top traverse.

## THIN SECTION 3-1



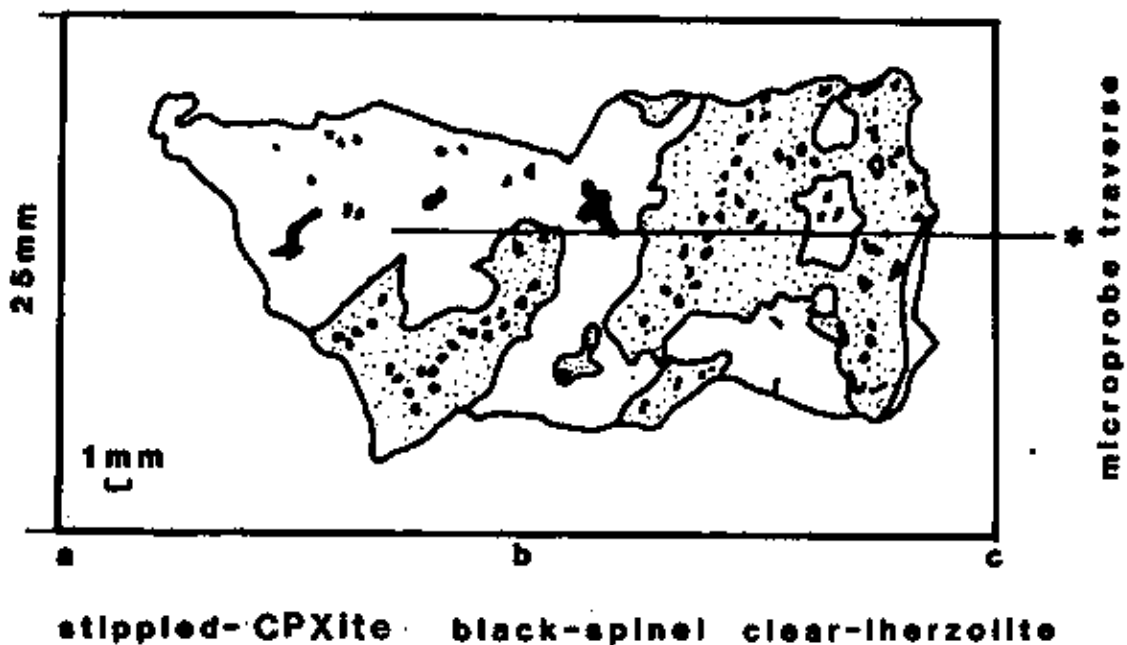
## Cr Content of Spinels



Cr levels in spinels

Figure 39.  $\text{Cr}_2\text{O}_3$  content of spinels,  
thin section SCB 383-6-2. Random distribution,  
only one traverse (\*).

## THIN SECTION 6-2

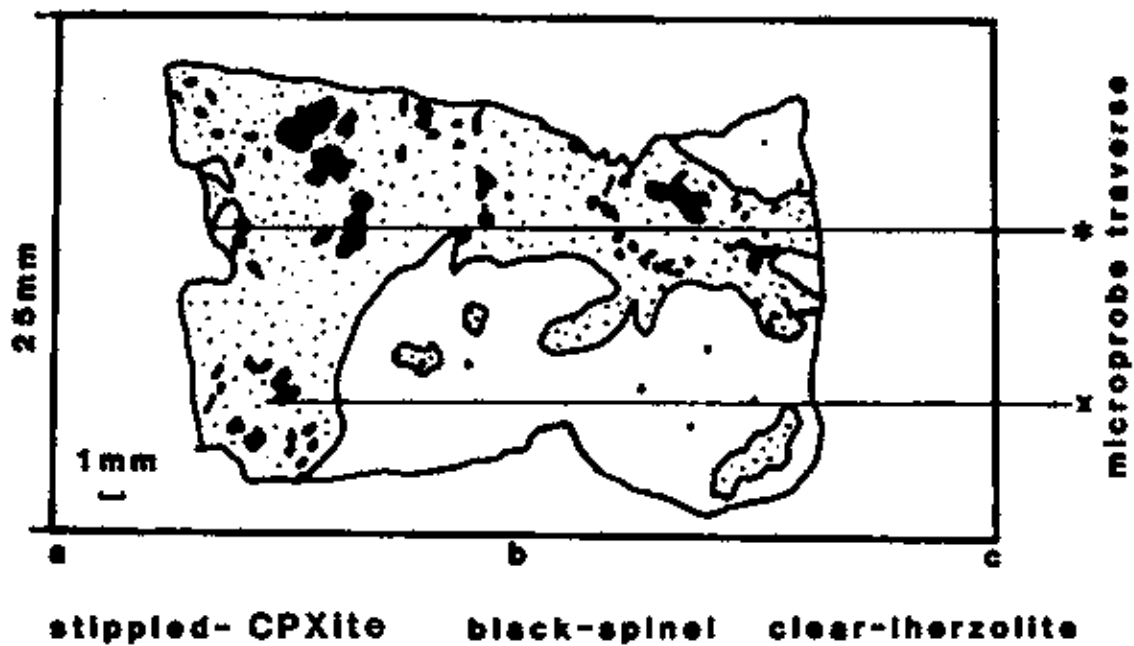


## Cr Content of Spinels



Figure 40.  $\text{Cr}_2\text{O}_3$  content of spinels,  
thin section SCB 383-6-3. Increase from left to  
right regardless of rock type. x represents bottom  
traverse, \* top traverse.

## THIN SECTION 6-3



## Cr Content of Spinels

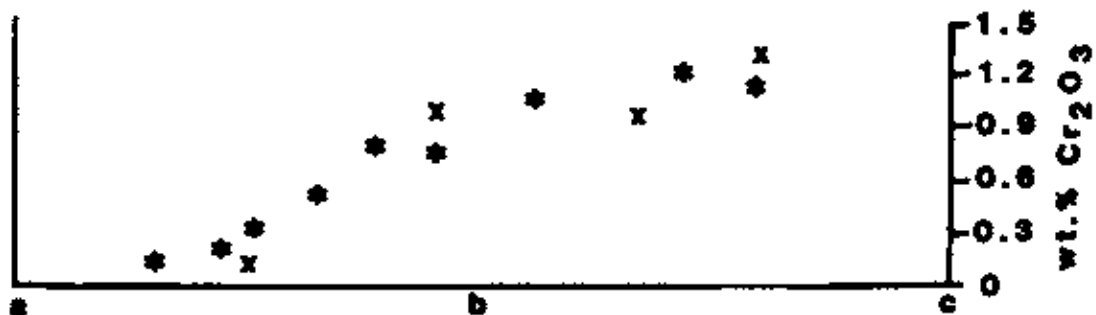
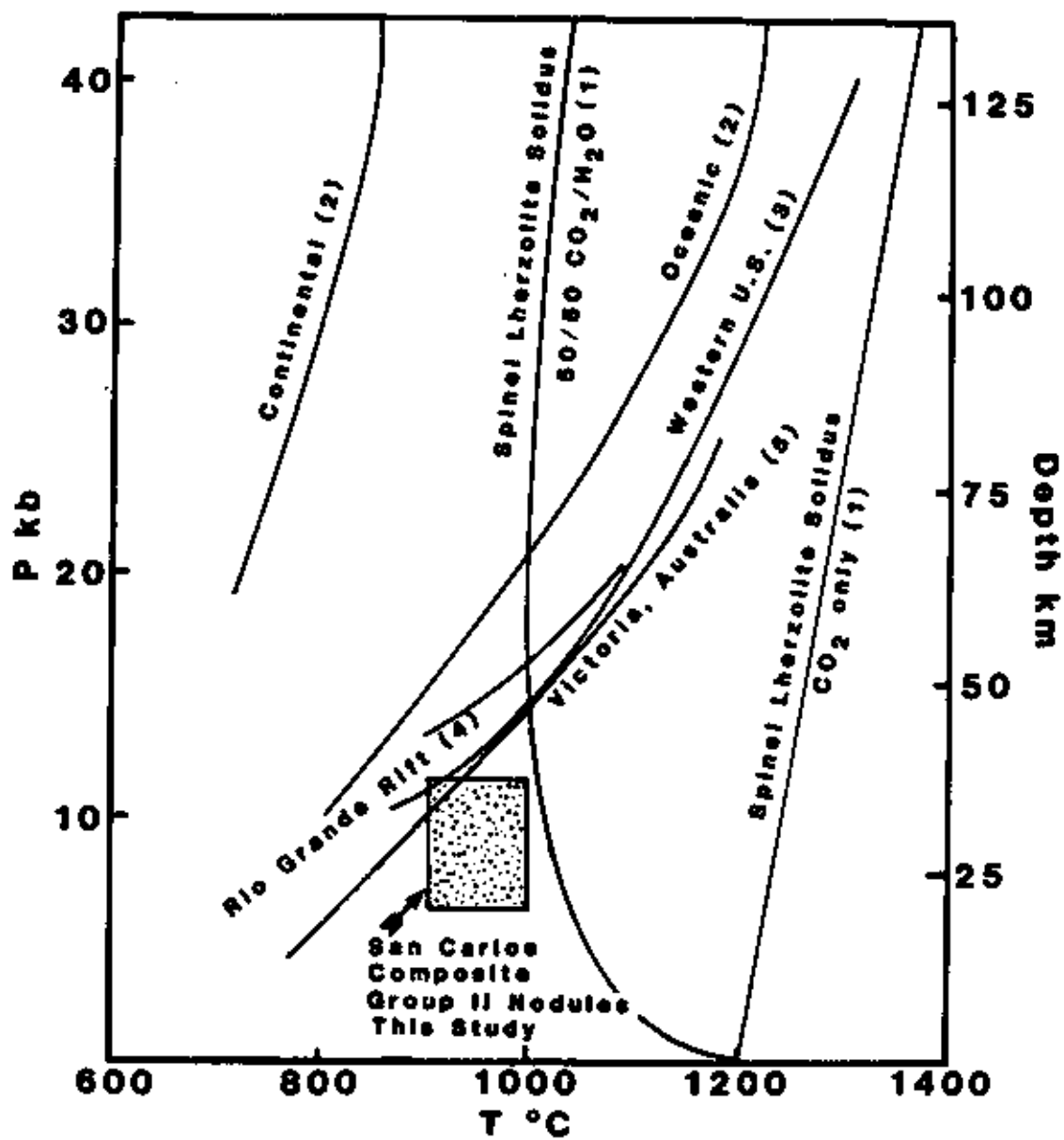


Figure 41. Geothermal gradients and envelope for Group II composite nodules from this study as determined from geothermometric and geobarometric calculations. These nodules plot to the high-temperature side of relevant geotherms, perhaps reflecting the influence of the vein-forming magma (hotter than "normal" temperatures). References: 1. various authors in Yoder, 1976; 2. Clark and Ringwood, 1964; 3. Mercier and Carter, 1975; 4. Reid, 1976; 5. Griffin et al., 1984.



## GEOOTHERMS

Figure 42. Drawing of  $ZrO_2$  cells as used at Temple University.

# TEMPLE UNIVERSITY IOF VERTICALLY OPPOSED DOUBLE CELL DESIGN

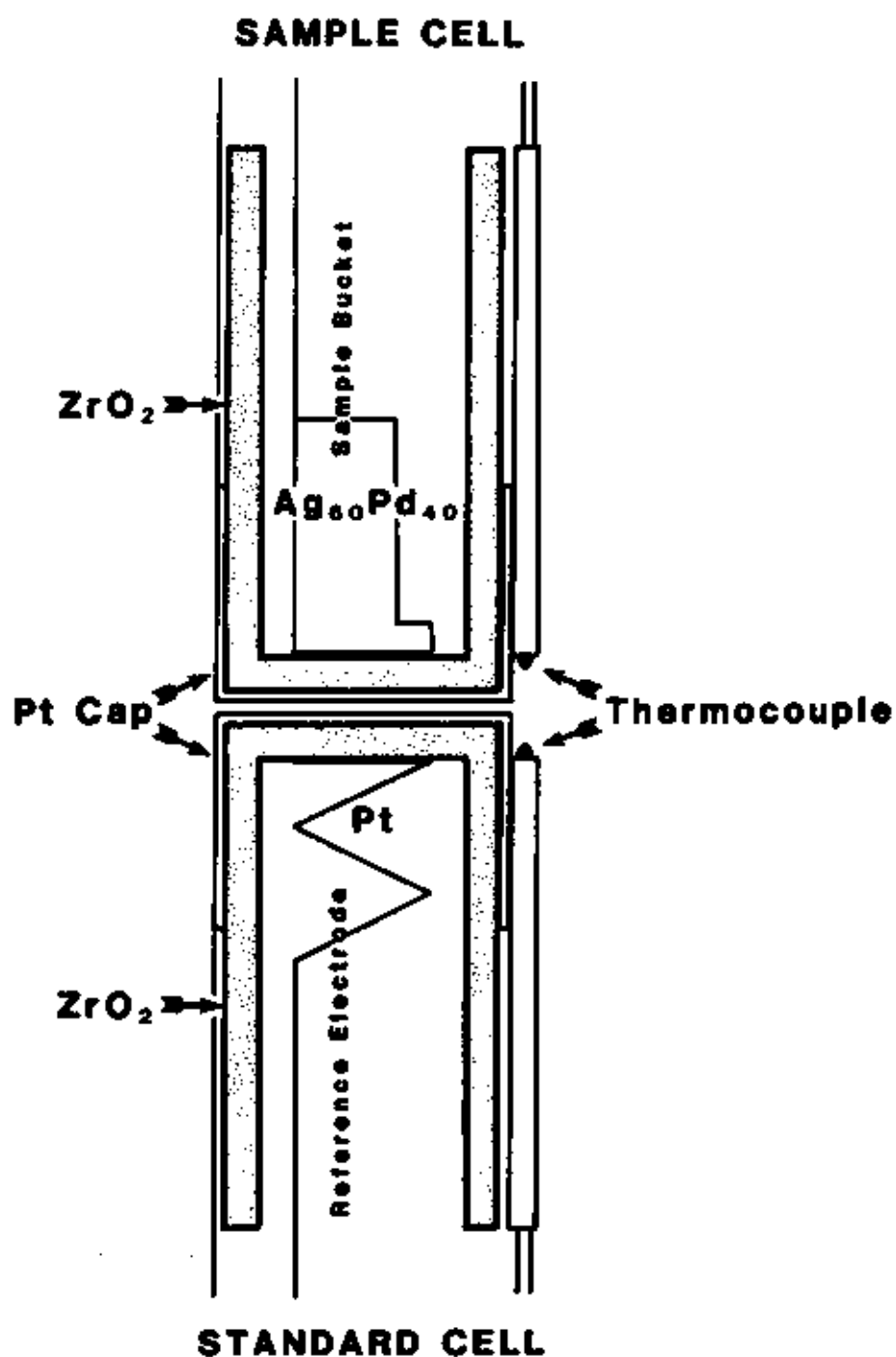


Figure 43. Schematic of Temple University IOF apparatus.

# SCHEMATIC OF TEMPLE IOF APPARATUS

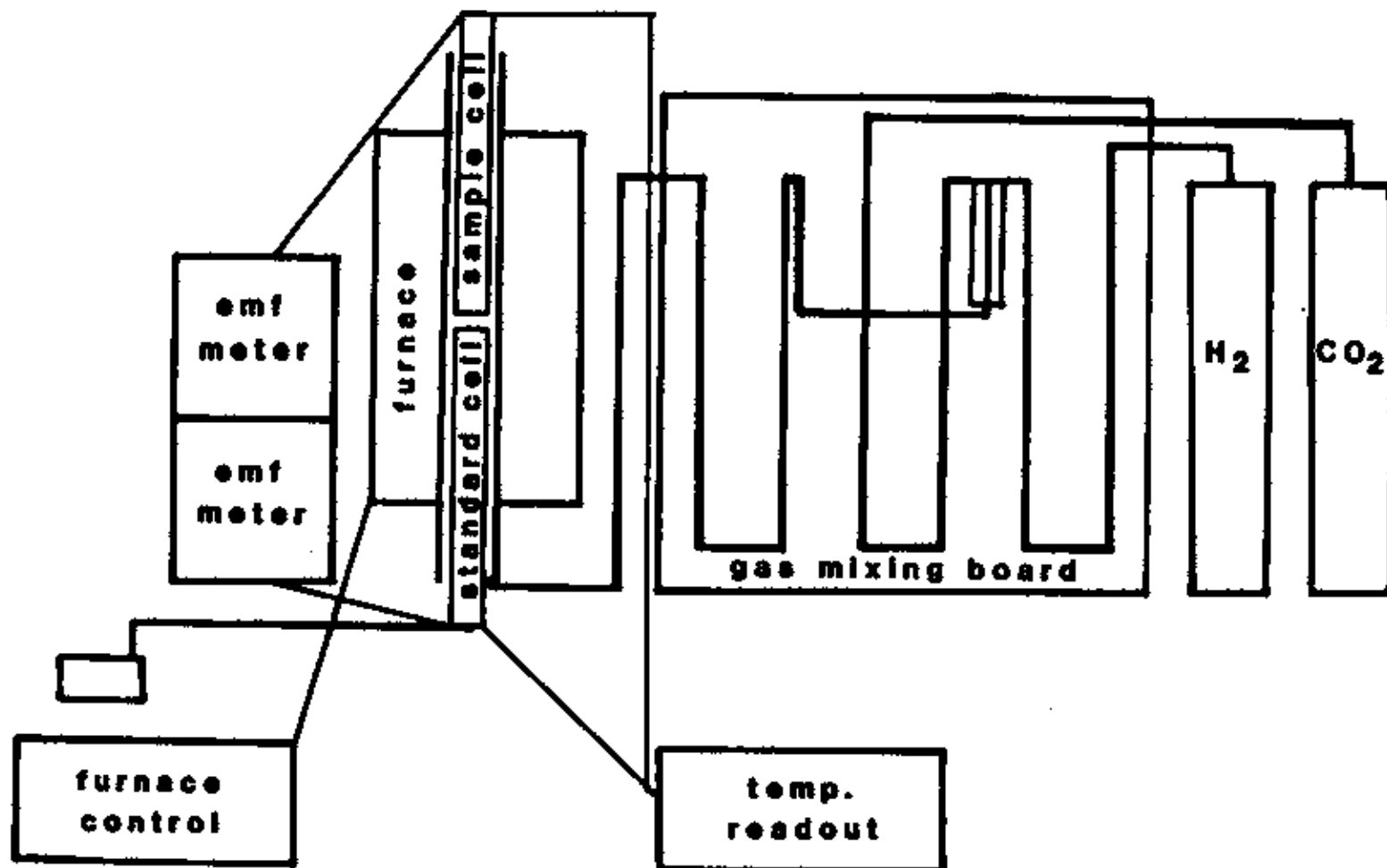


Figure 44. IOF data points and curve: SCB 383-3-olivine.  
17 data points  
LSF equation:  $78.585 + 3.053 x = Y$   
 $X = 1/T^{\circ}K \times 10^4$ ,  $Y = -\log fO_2$   
Standard error: 0.700

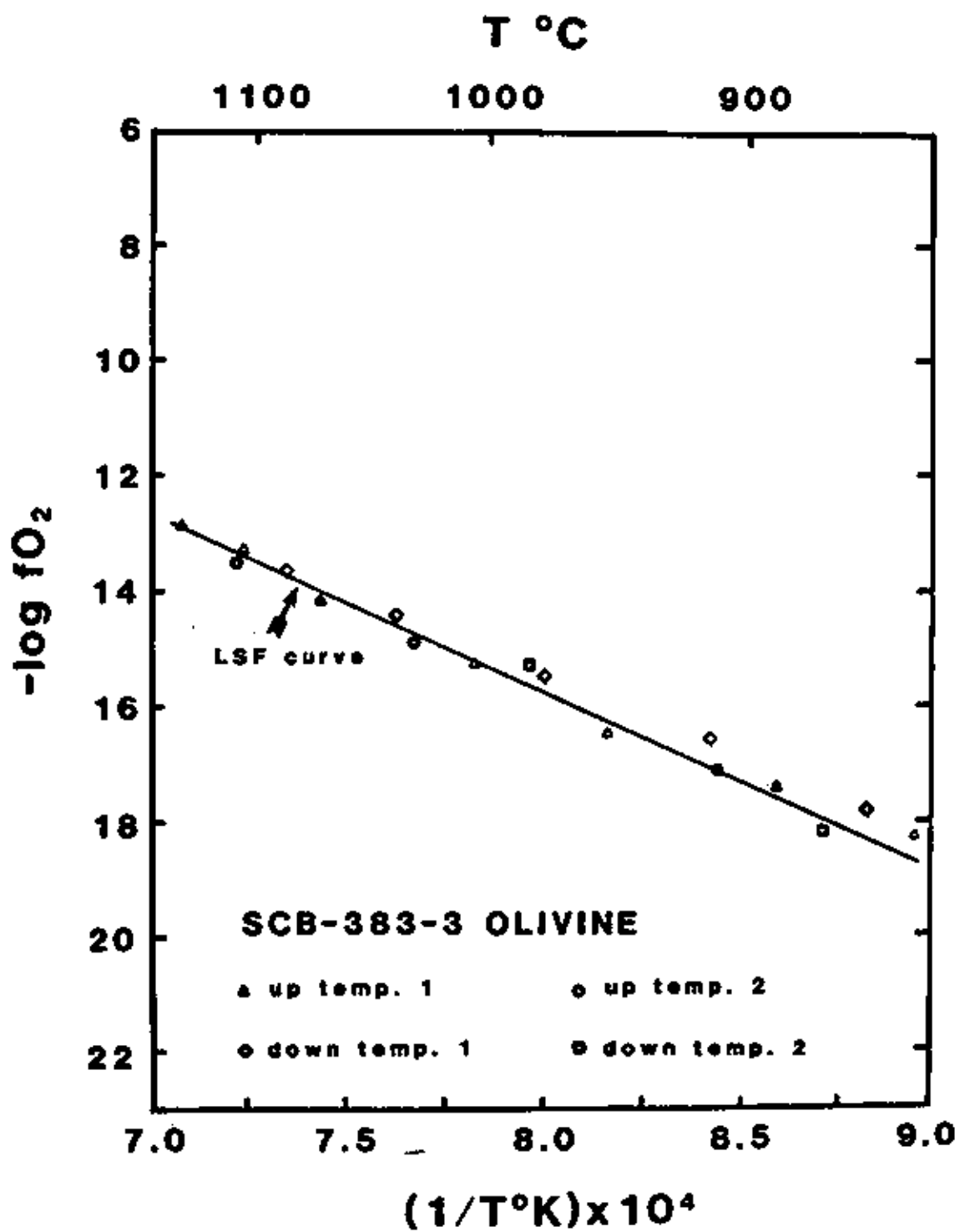


Figure 45. IOF data and curve: SCB 383-3-CPX  
LSF equation:  $712.106 + 3.234 X = Y$   
 $X = 1/T^{\circ}K \times 10^4$ ,  $Y = -\log fO_2$   
12 data points  
Standard error: 0.886

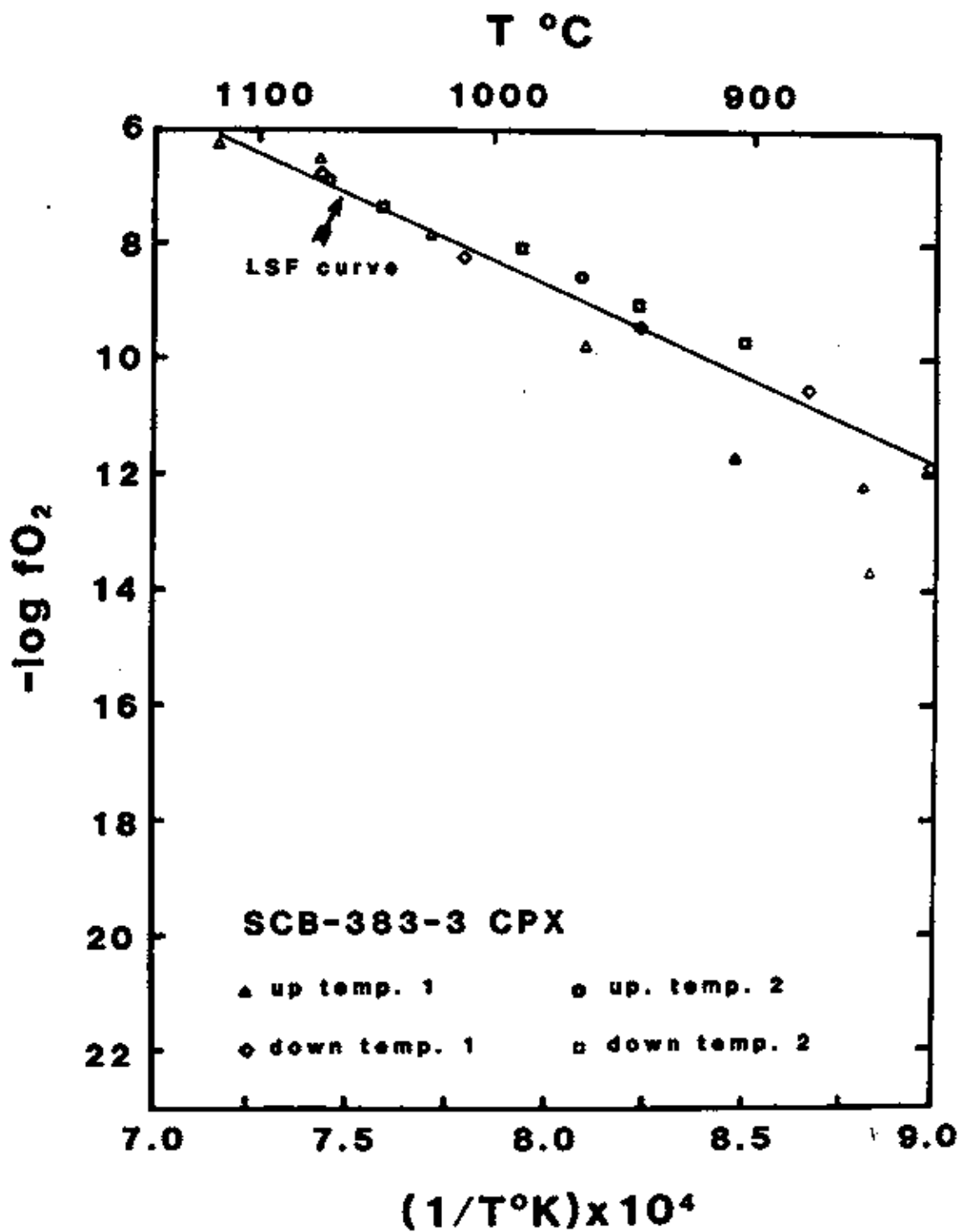


Figure 46. IOF data and curve: SCB 383-2-olivine  
LSF equation:  $712.106 + 3.234 X = Y$   
 $X = 1/T^{\circ}K \times 10^4$ ,  $Y = -\log fO_2$   
12 data points  
Standard error: 0.886

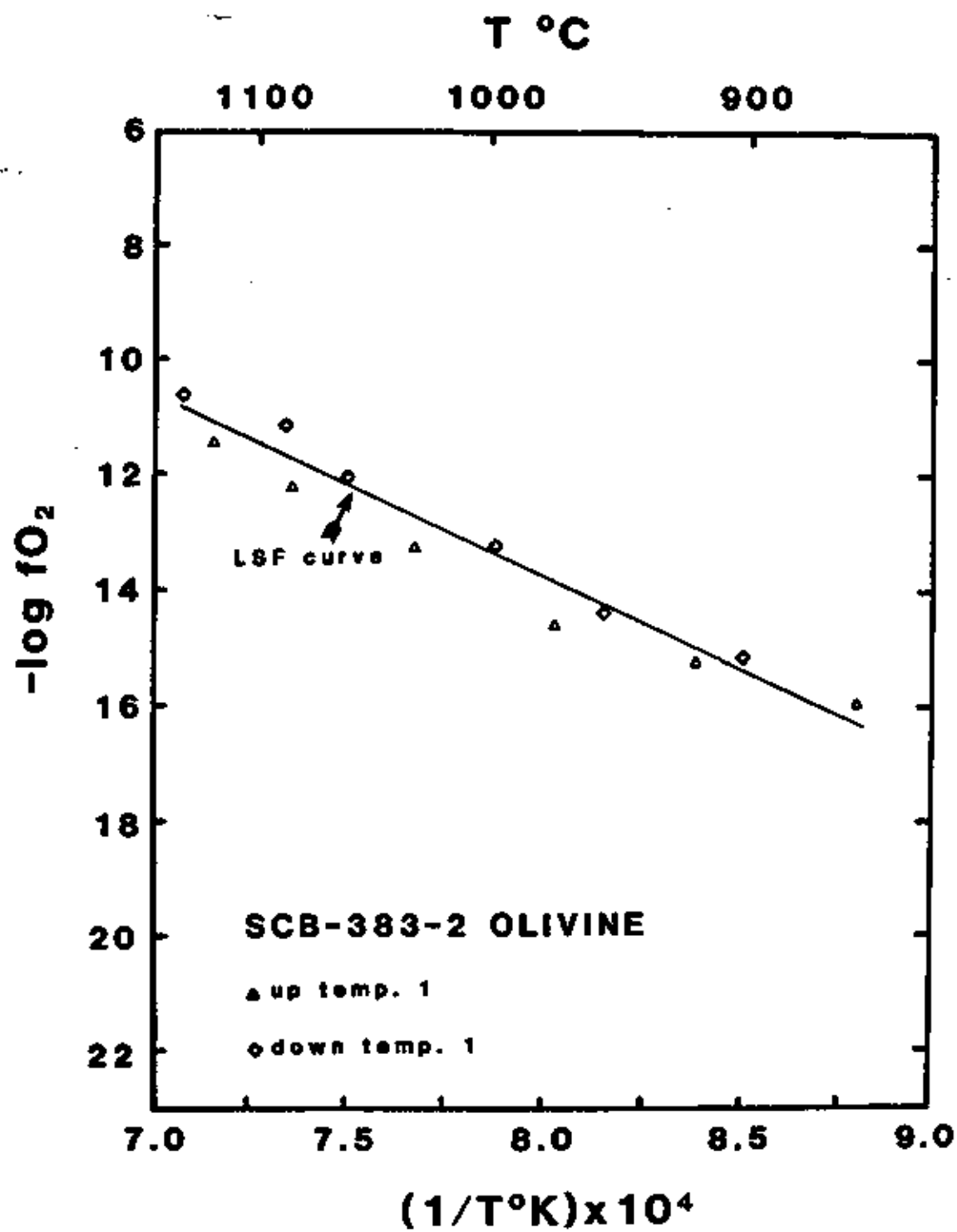


Figure 47. IOP data and curve: SCB 383-2-CPX.  
LSF equation:  $711.93 + 3.247 X = Y$   
 $X = 1/T^{\circ}K \times 10^4$ ,  $Y = -\log fO_2$   
15 data points  
Standard error: 0.648

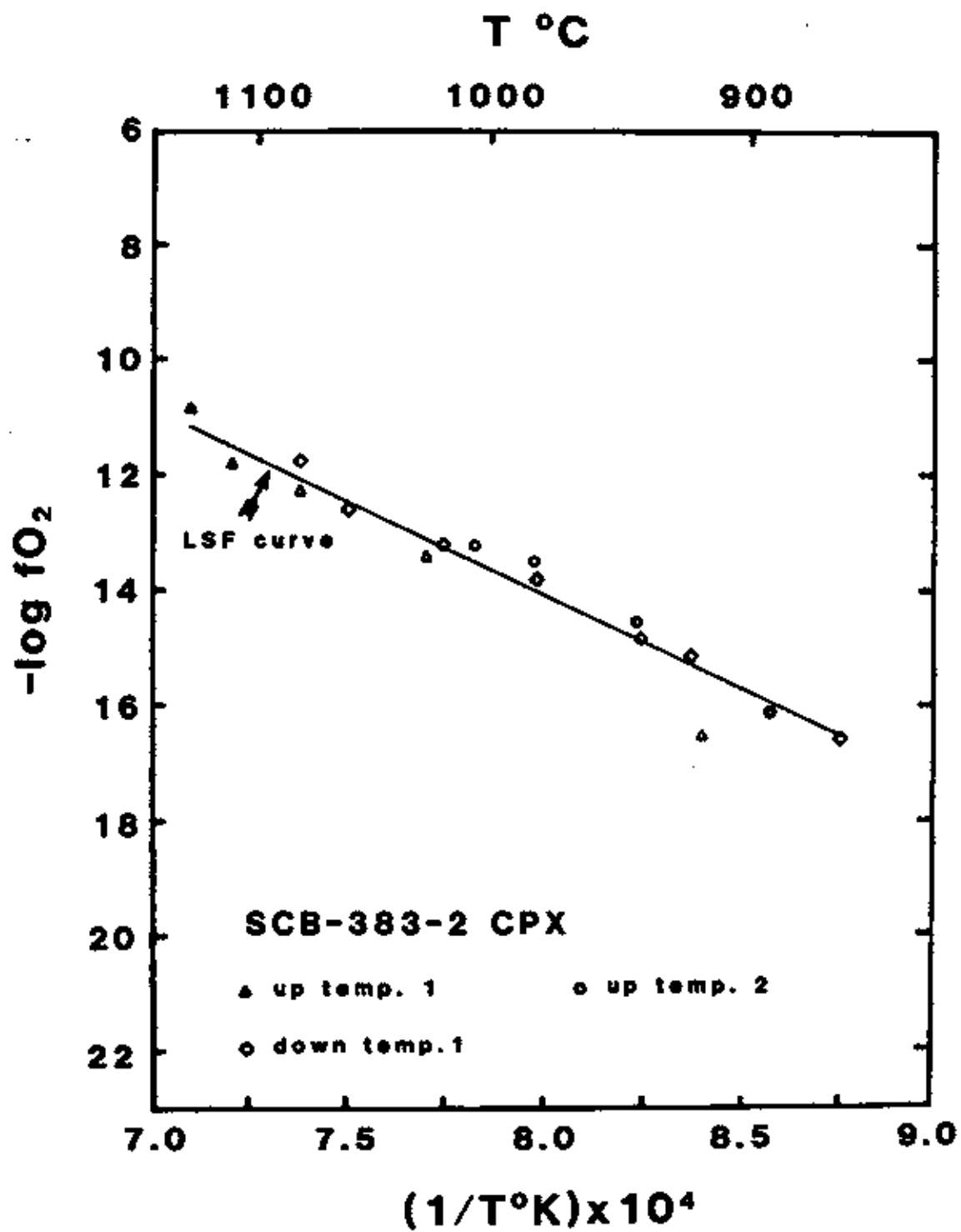


Figure 48. IOF data and curve: SCB 383-2-spinel.  
LSF equation:  $10.613 + 3.253 X = Y$   
 $X = 1/T^{\circ}K \times 10^4$ ,  $Y = -\log fO_2$   
17 data points  
Standard error: 0.780

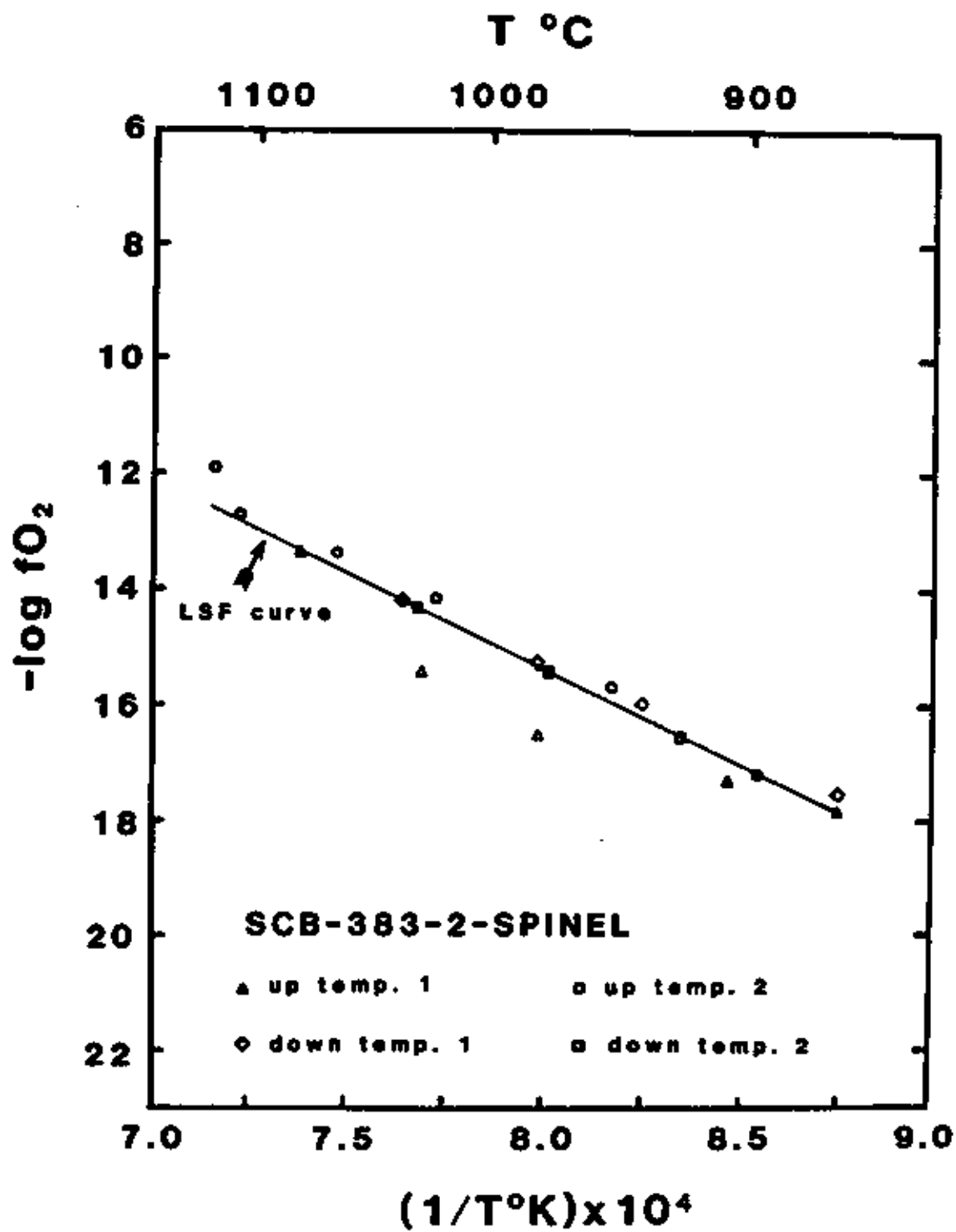


Figure 49. IOF data curves for composite Group II nodule minerals, this study, Temple and Reston analyses.

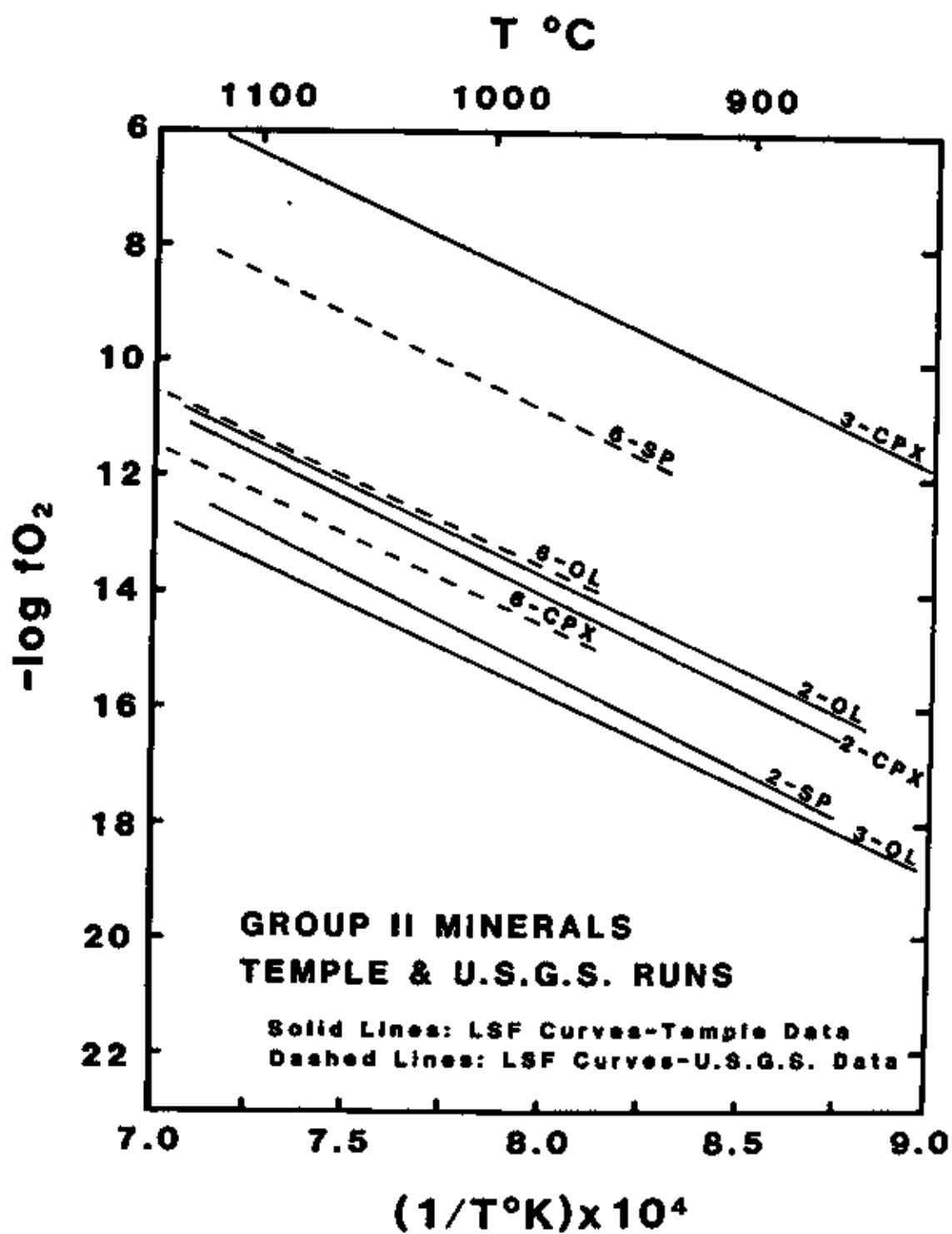


Figure 50. IOF data and curve, Group I olivine, Koseluk  
(1979).

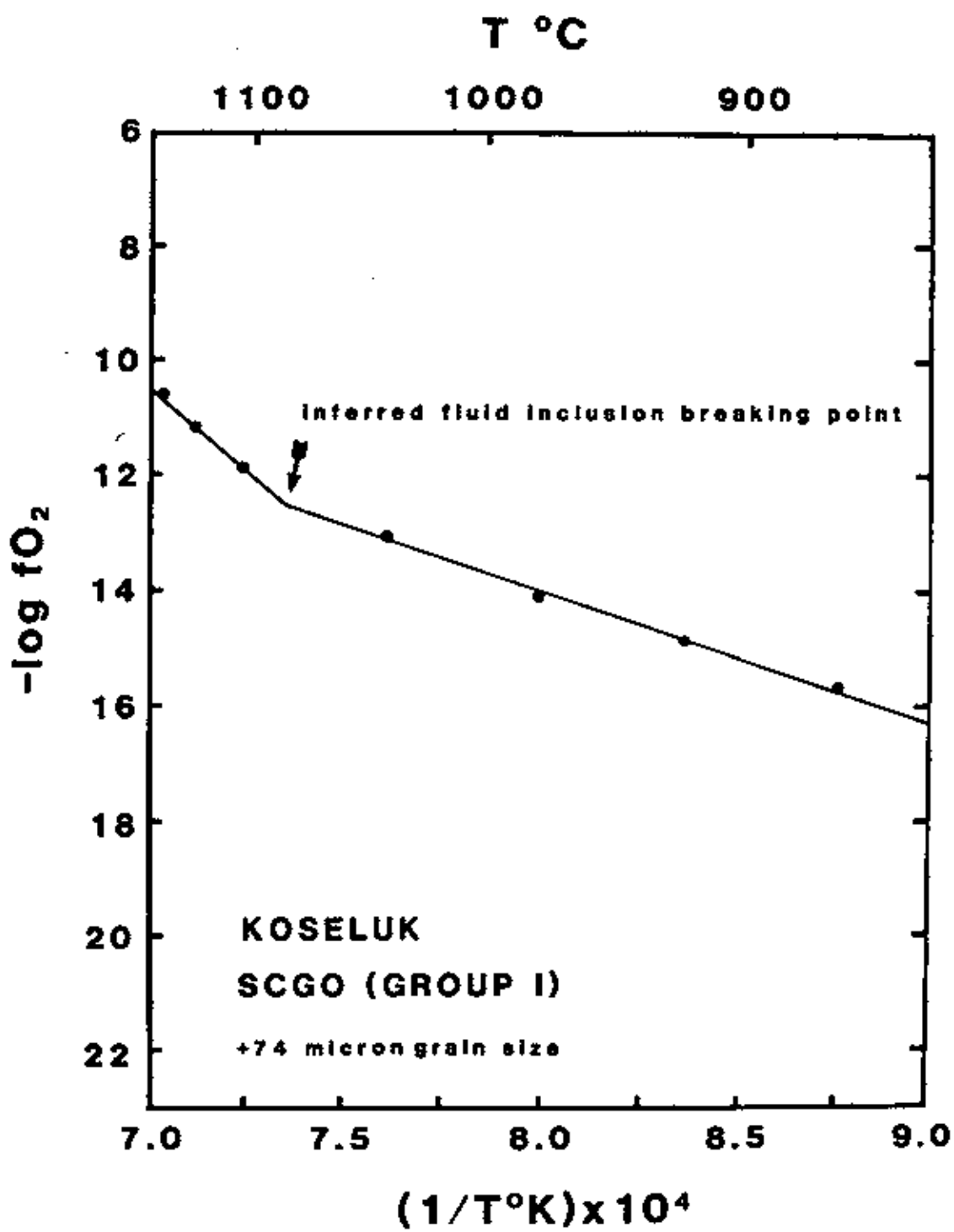
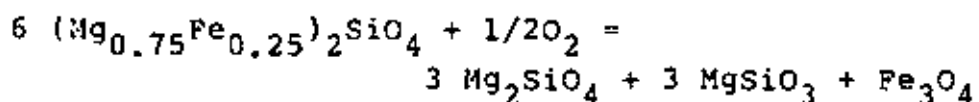


Figure 50a. IOF curves for Group II minerals and an approximation of the upper limit of the stability field for olivine: Fo-75. This limit was calculated from the reaction:



using data from Robie et. al., (1979). This reaction for the oxidation of Fo-75 was suggested by XRD analysis of Fo-77 olivine oxidized during TGA.

Note that two of the olivine IOF curves intersect the phase boundary within the diagram, while the third can be projected to intersect at 1260°C. The intersections suggest that the IOF curves for the olivine were not determined by the olivine, but rather, were controlled by some other phase (i.e., CO<sub>2</sub>).

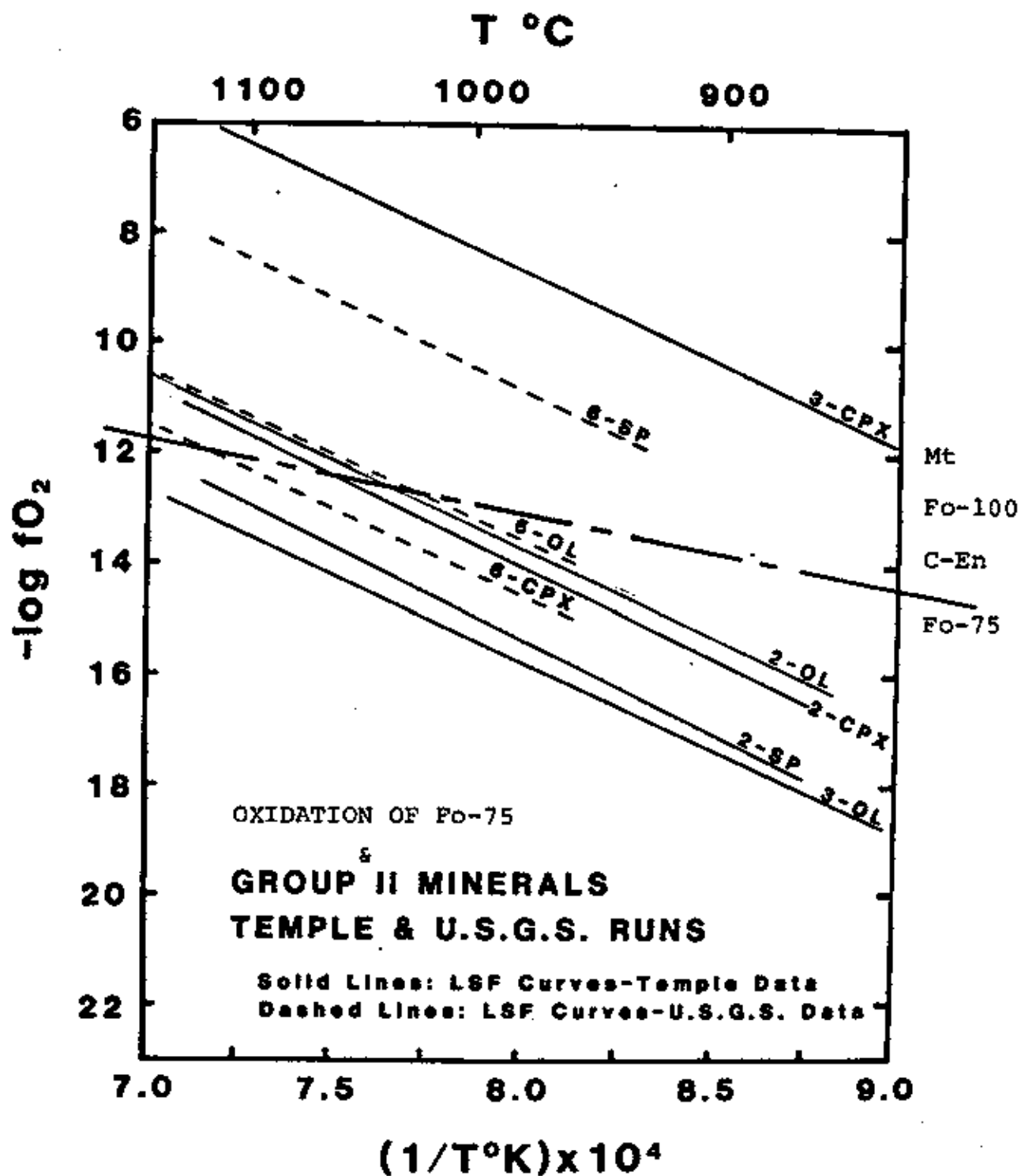
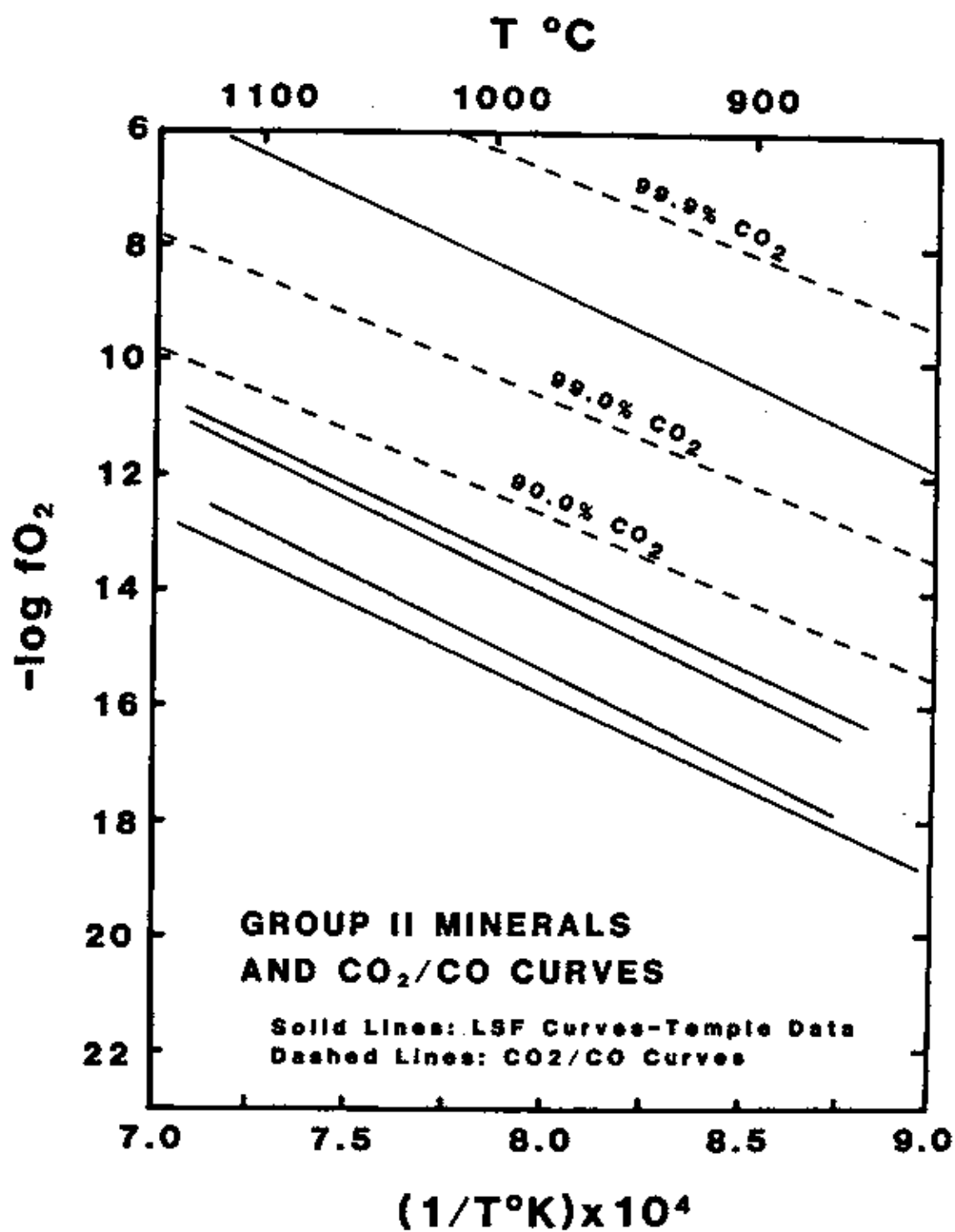


Figure 51. IOF data curves, Group II minerals, Temple analyses, and  $\text{CO}_2/\text{CO}$  curves (Deines et al., 1974). The deviation from parallelism between Group II minerals and the gas curves suggests that the IOF of the host solid phases may have contributed to the IOF of the  $\text{CO}_2$  released from fluid inclusions during analyses.



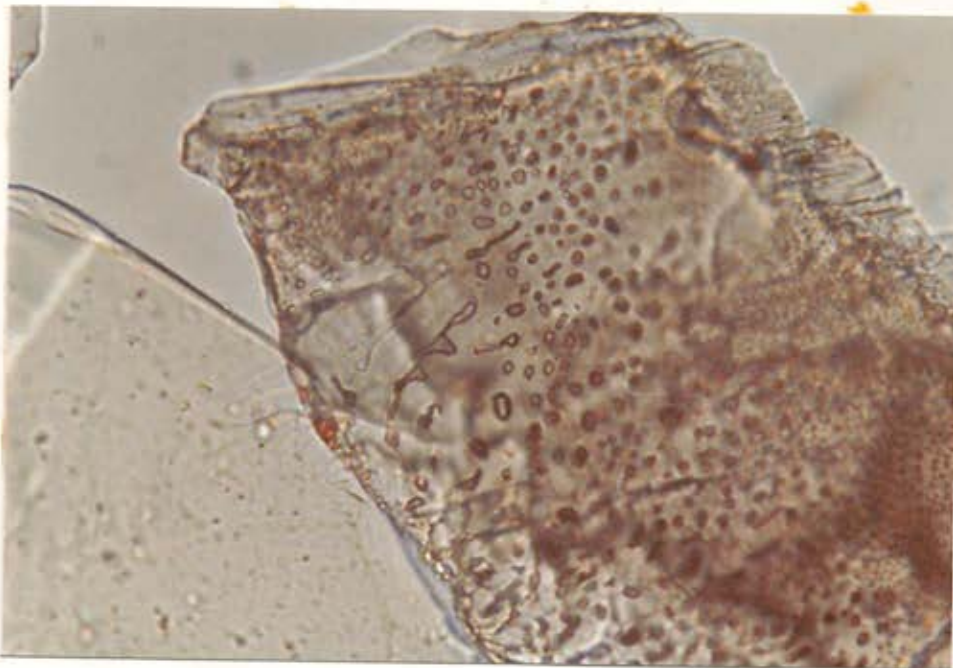


Figure 52. Fluid inclusions in Group II olivine. Note the large size (some near 5 microns) and deformation (necking) of some inclusions. PPL, 210 x 150 microns.

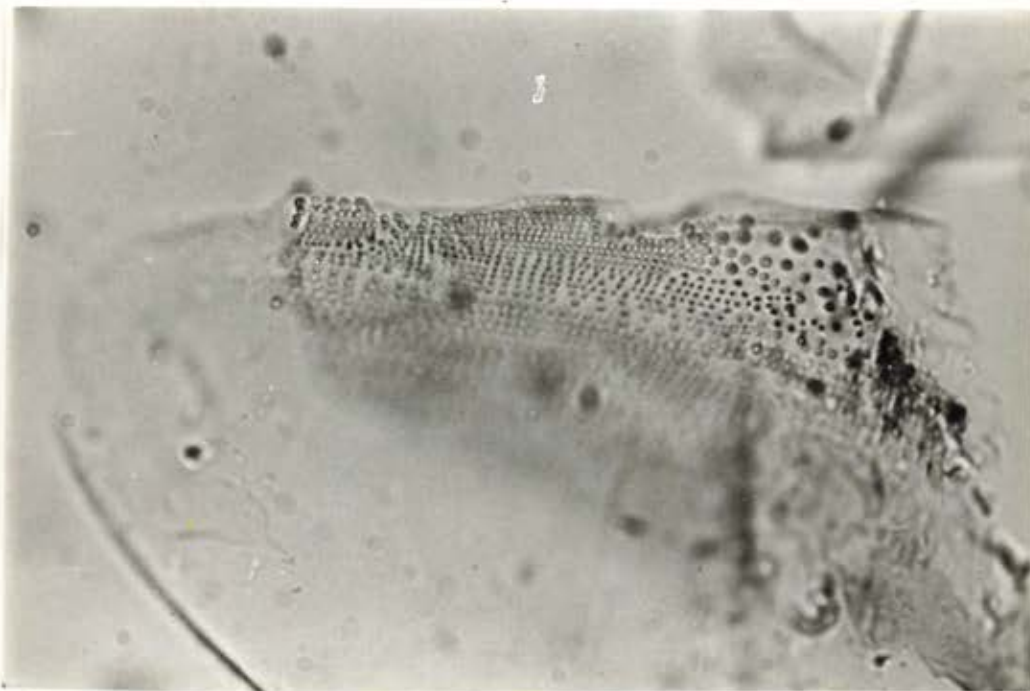


Figure 53. Fluid inclusions in Group II olivine. PPL, 210 x 150 microns.


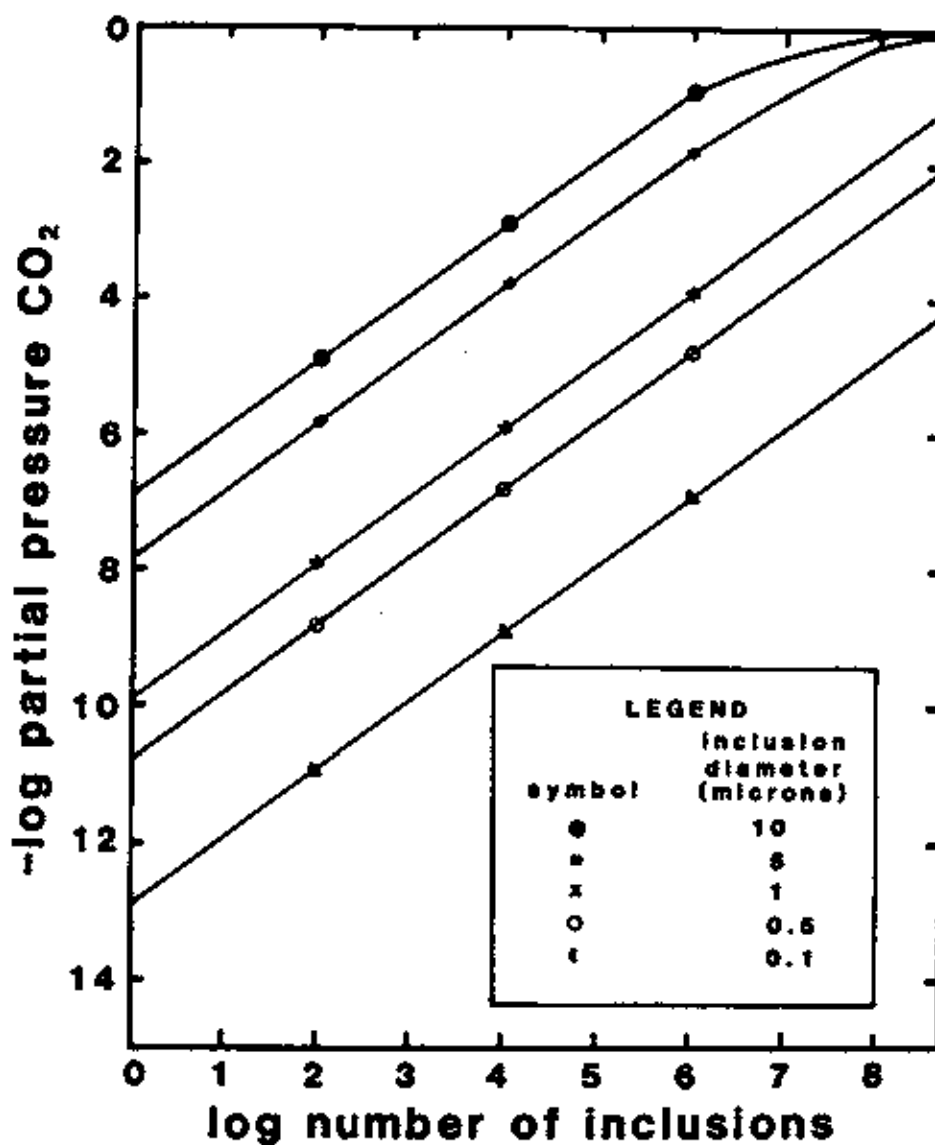


Figure 54. Numbers of  $\text{CO}_2$  inclusions against  $p\text{CO}_2$  generated by their breaking and liberating their contents at  $1000^\circ\text{C}$  ( $1273^\circ\text{K}$ ) inside the argon-filled  $2\text{ cm}^3$  free space of the  $\text{ZrO}_2$  IOF sample cell. The slope change in the 10 and 5 micron curves represents the asymptotic approach of  $p\text{CO}_2$  to 100%.



**$\text{CO}_2$  INCLUSIONS vs PARTIAL PRESSURE  $\text{CO}_2$**   
**IOF CELL - 2  $\text{cm}^3$  FREE SPACE**  
**1273° K**

Figure 55.  $fO_2$  of  $CO_2$  released from 1 micron inclusions as a function of numbers of inclusions and temperature.

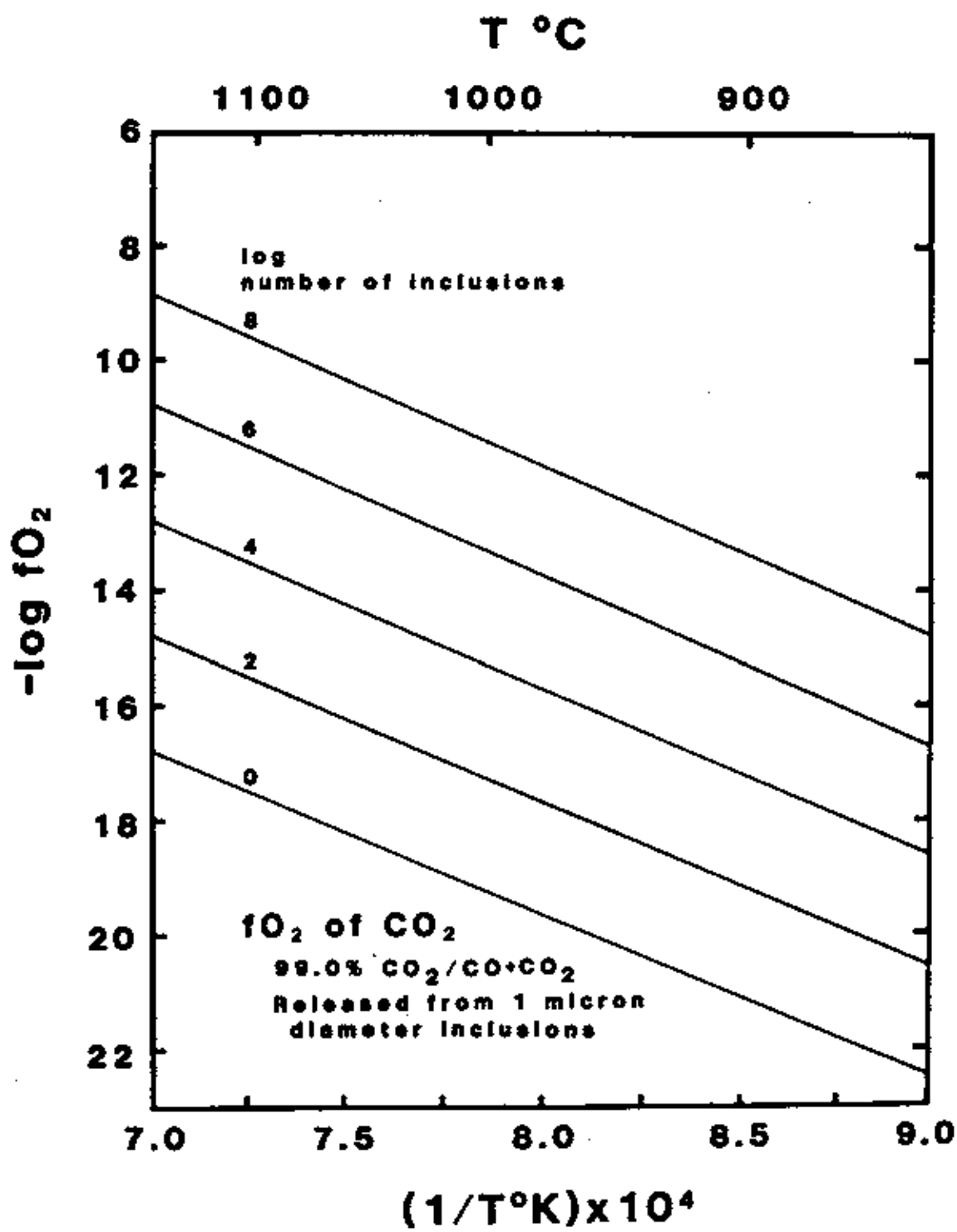
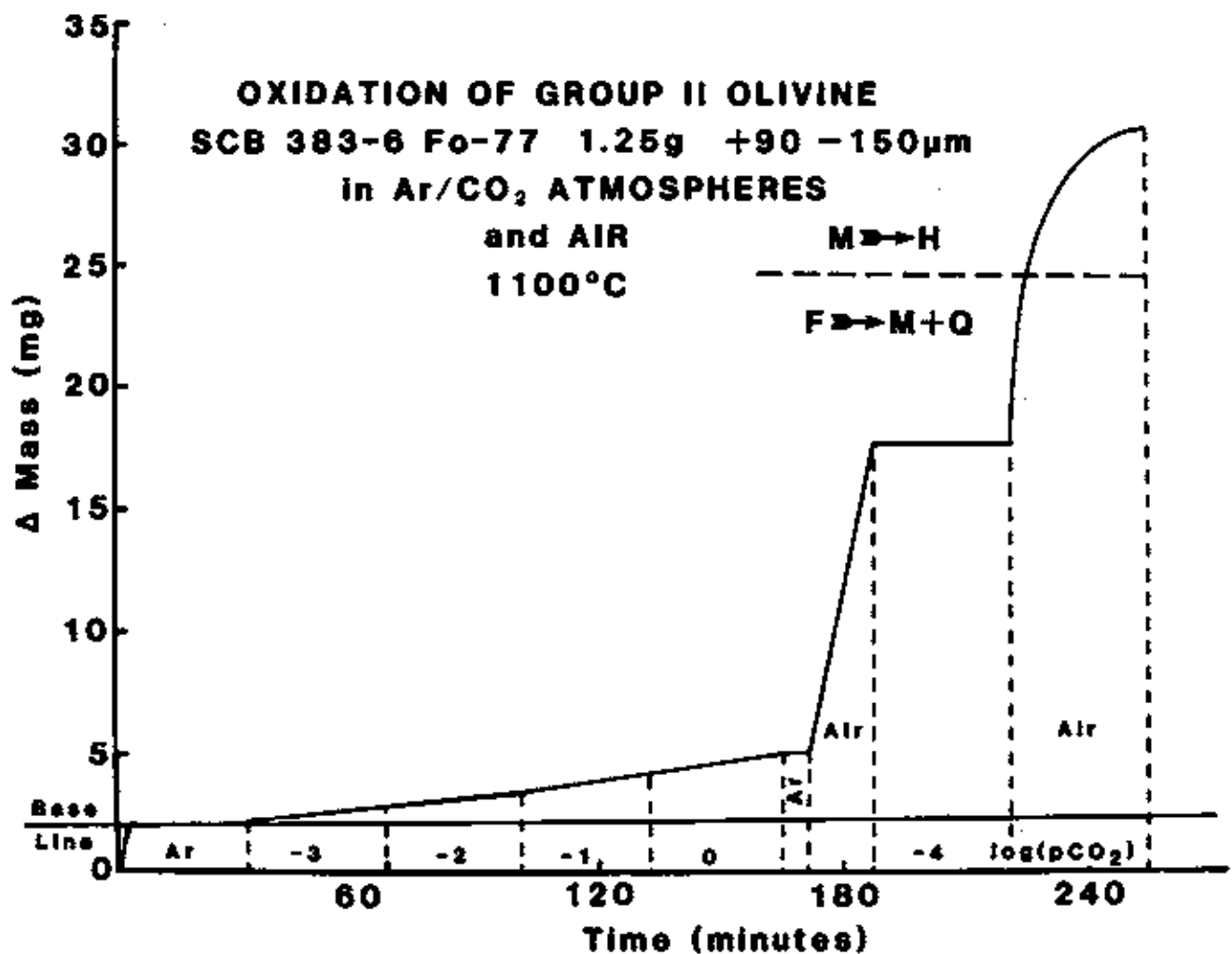


Figure 56. Results of TGA of Fo-77 Group II San Carlos olivine. Horizontal dashed line represents the fayalite (F→MQ)/magnetite (M→H) boundary.



**THERMOGRAVIMETRIC ANALYSIS**

Figure 57. Group II IOF values and curves for  $p\text{CO}_2$  values of  $10^{-3}$  and  $10^{-4}$ , i.e., values bracketing  $p\text{CO}_2$  below which olivine (Fo-77) does not oxidize. Note that all but one of the curves plots below the reaction curve if the presumed Reston oxidation error is eliminated.

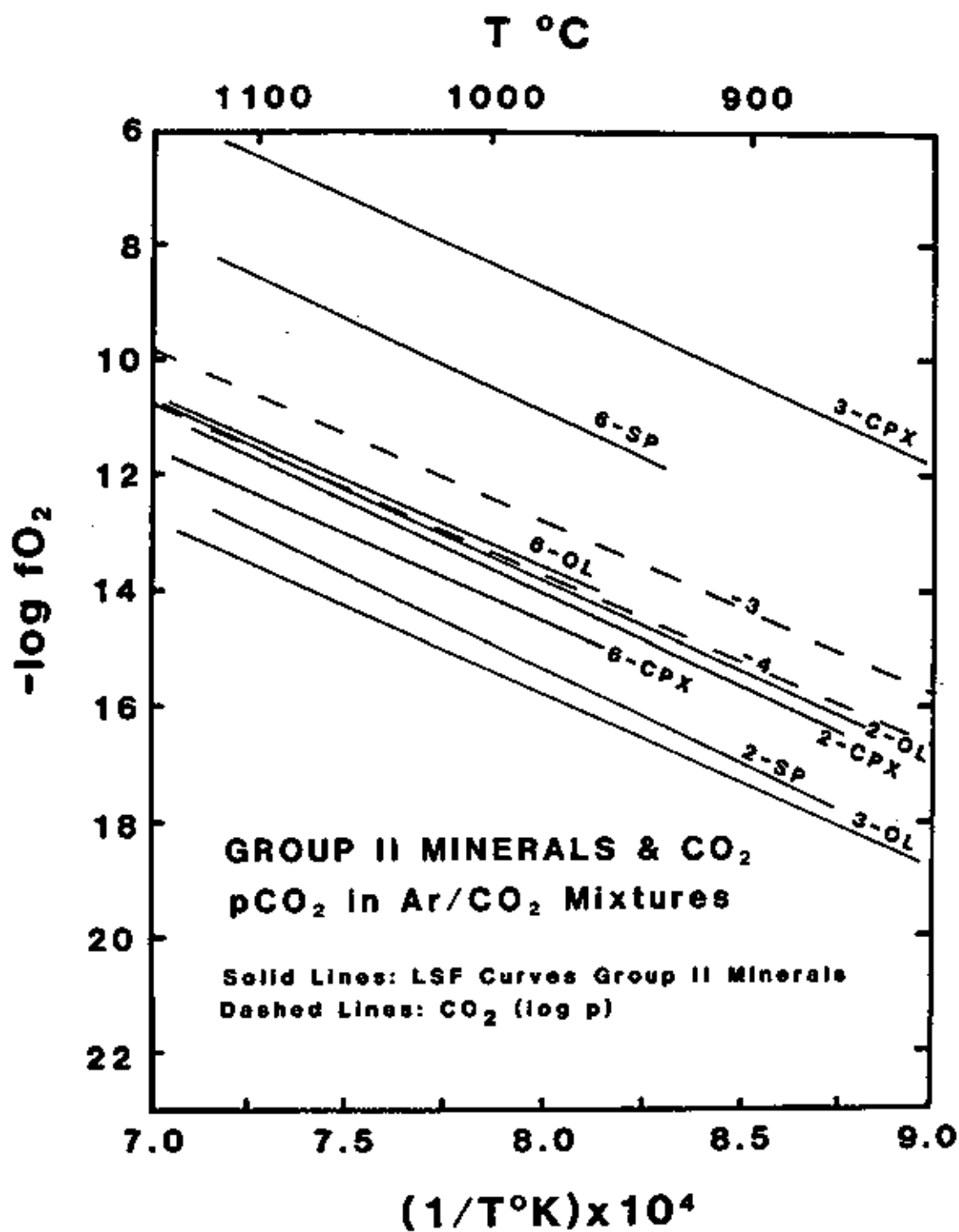


Figure 58. IOF curves for Group II minerals, Temple analyses, and Arculus et al. envelopes for Group I and Group II nodules. The Group II envelope also encloses values for ilmenite megacrysts. Note that only one of the curves plot within the Arculus et al. Group II envelope. This is from a Reston analysis and will plot below the envelope if the presumed error is eliminated.

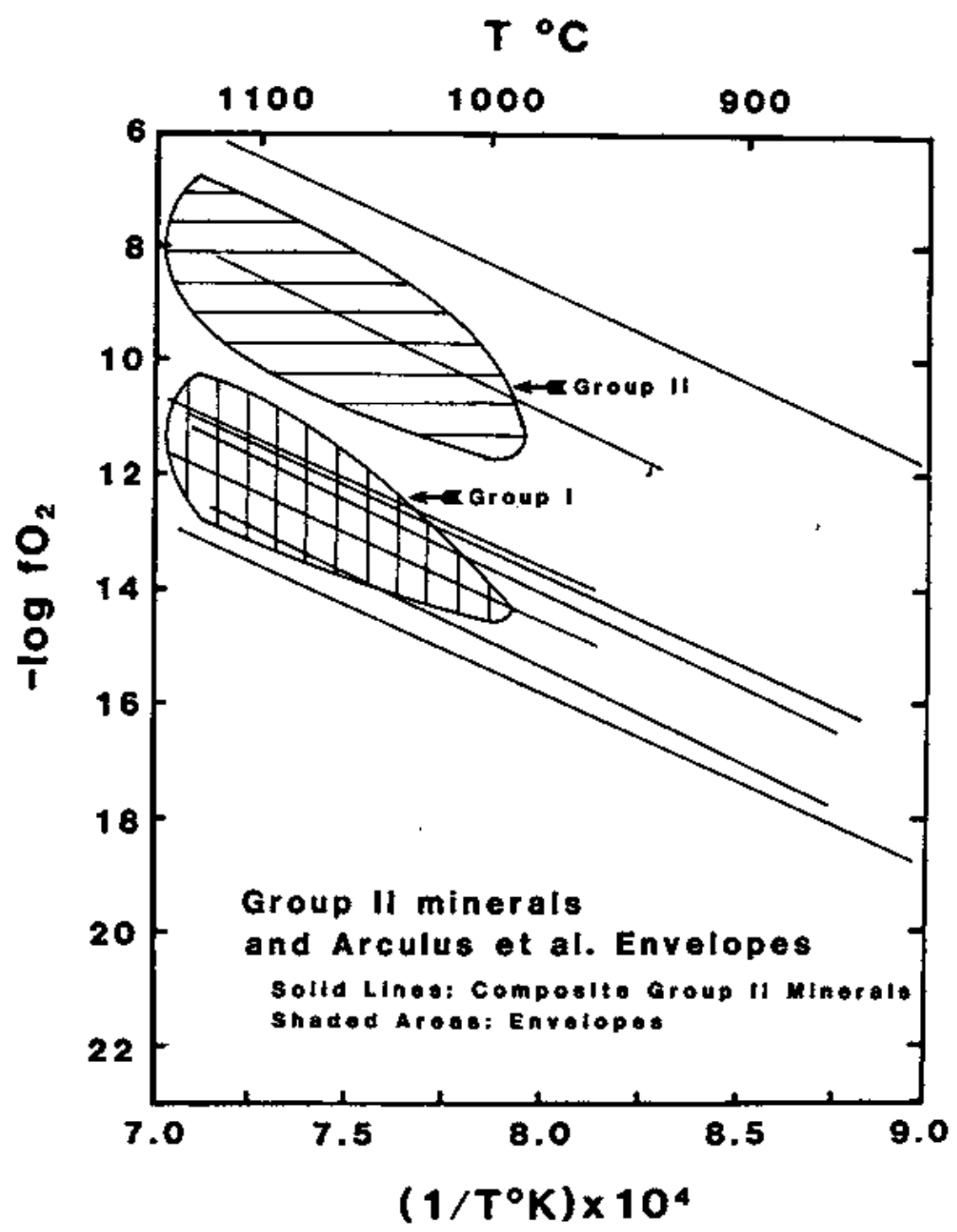
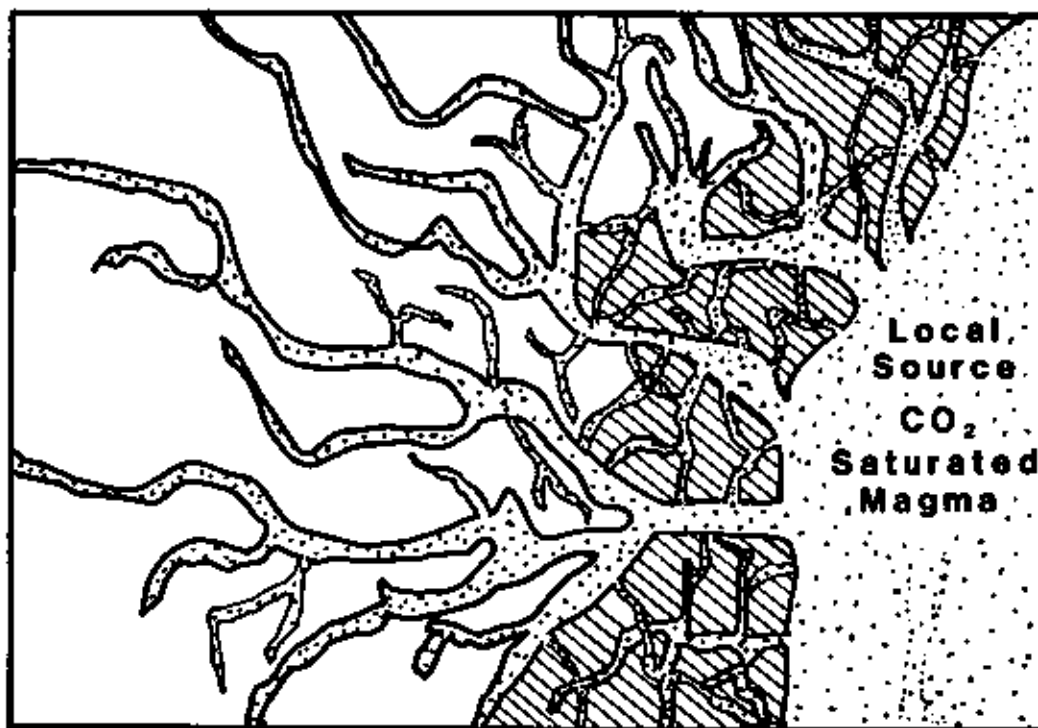


Figure 59. Model for the upper mantle in regions of vein intrusion that resulted in the formation of rocks ultimately brought to the surface as Group I or Group II composite xenoliths with Group II veins.

LESS ————— **Subsolidus Processes** ————— MORE

LESS ————— **Homogenization** ————— MORE  
(WITH RESPECT TO VEIN/WALL-ROCK RELATIONSHIPS)



CLEAR: GROUP I LHERZOLITE                      STIPPLED: WEHLITE  
HACHURED: GROUP II LHERZOLITE

**CROSS-SECTION OF UPPER-MANTLE SOURCE REGION  
FOR COMPOSITE NODULES WITH WEHLITE VEINS**

TABLE I

## REPRESENTATIVE MICROPROBE DATA

	OLIVINE				
	Nodule Sample	1 1-2A	2 1-4A	6 3-5B	Group I 4-C
Wt%					
MgO		37.86	41.28	39.69	49.71
SiO <sub>2</sub>		38.17	39.57	38.28	40.26
FeO		24.11	19.67	21.37	9.92
CaO		0.12	0.12	0.13	0.09
NiO		0.17	0.20	0.27	0.24
MnO		0.26	0.20	0.22	0.20
Total		100.69	101.04	99.96	100.42

	CLINOPYROXENE				
	Nodule Sample	1 1-7B	2 1-3B	6 1-1A	Group I F&P-PA6
Na <sub>2</sub> O		1.00	0.85	1.06	2.01
MgO		13.09	13.77	13.37	16.20
Al <sub>2</sub> O <sub>3</sub>		7.75	7.57	7.84	6.20
SiO <sub>2</sub>		48.02	48.82	48.19	50.80
CaO		20.81	20.86	20.67	19.50
TiO <sub>2</sub>		1.55	1.31	1.60	0.22
Cr <sub>2</sub> O <sub>3</sub>		0.06	0.15	0.15	1.29
MnO		0.08	0.04	0.07	0.05
FeO		7.09	6.07	6.10	2.88
Total		99.46	99.55	99.05	99.15

TABLE I (cont.)

	Nodule Sample	SPINEL			Group I GEN-1
		1 1-H	2 2-A	3 1-K	
Wt %					
MgO		16.29	18.32	16.39	18.21
Al <sub>2</sub> O <sub>3</sub>		60.32	60.62	56.55	34.00
FeO		16.92	13.38	16.06	10.93
Fe <sub>2</sub> O <sub>3</sub>		5.62	5.51	6.18	4.48
Cr <sub>2</sub> O <sub>3</sub>		0.45	1.28	4.43	33.29
MnO		0.18	0.16	0.32	0.72
TiO <sub>2</sub>		0.48	0.33	0.56	0.33
Total		100.52	99.75	100.84	100.78

TABLE II

## AVERAGE COMPOSITION OF MINERAL PHASES IN 4 NODULES

		OLIVINE							
Nodule	1	2		3		6			
# data points	8	10		7		28			
Wt%	x	s	x	s	x	s	x	s	
MgO	38.74	0.67	41.51	0.60	40.19	0.66	39.73	0.60	
SiO <sub>2</sub>	37.93	0.49	39.23	0.76	38.63	0.29	38.47	0.47	
FeO	22.79	0.67	19.20	0.31	21.87	0.53	21.42	0.71	
Total	100.06	0.62	100.41	0.89	101.21	0.88	100.42	0.71	

		CLINOPYROXENE							
Nodule	1	2		3		6			
# data points	4	6		4		8			
Wt%	x	s	x	s	x	s	x	s	
Na <sub>2</sub> O	1.07	0.05	0.90	0.16	1.11	0.06	1.08	0.11	
MgO	12.85	0.19	14.05	0.18	13.35	0.18	13.44	0.17	
Al <sub>2</sub> O <sub>3</sub>	8.21	0.33	7.72	0.21	8.05	0.13	7.95	0.20	
CaO	20.41	0.44	20.73	0.17	20.03	0.18	20.11	0.24	
FeO	7.20	0.17	5.93	0.23	6.74	0.20	6.27	0.17	
SiO <sub>2</sub>	47.22	0.62	48.21	0.44	48.13	0.22	48.09	0.35	
Total	98.97	0.70	99.11	0.42	98.96	0.26	99.29	0.25	

TABLE II (cont.)

SPINEL									
Nodule	1		2		3		6		
# data points	19		19		19		22		
Wt%	x	s	x	s	x	s	x	s	
MgO	16.16	0.31	18.22	0.26	16.73	0.38	17.51	0.43	
Al <sub>2</sub> O <sub>3</sub>	59.04	0.88	60.84	0.79	59.15	1.42	60.67	1.32	
Cr <sub>2</sub> O <sub>3</sub>	0.44	0.23	0.97	0.36	2.33	1.33	1.28	0.62	
sum Fe	22.34	0.72	18.39	0.45	20.82	0.58	19.01	0.39	
FeO	16.55	0.34	13.48	0.65	15.90	0.40	14.53	1.10	
Fe <sub>2</sub> O <sub>3</sub>	6.49	0.71	5.52	0.73	5.46	0.43	4.95	0.93	
TiO <sub>2</sub>	0.48	0.06	0.33	0.03	0.46	0.06	0.36	0.04	
Total	99.72	0.97	99.76	0.72	100.76	1.04	100.02	0.98	

TABLE III

AVERAGE MINERAL COMPOSITIONS  
4 NODULES TAKEN AS 1 POPULATION

OLIVINE		
n=45		
Wt%	x	s
MgO	39.94	1.15
SiO <sub>2</sub>	38.42	0.63
FeO	21.38	1.40
Total	100.42	0.55

CLINOPYROXENE		
n=22		
Wt%	x	s
Na <sub>2</sub> O	1.03	0.13
MgO	13.48	0.44
Al <sub>2</sub> O <sub>3</sub>	7.96	0.28
CaO	20.42	0.36
SiO <sub>2</sub>	48.00	0.53
FeO	6.43	0.49
Total	99.10	0.40

SPINEL		
n=79		
Wt%	x	s
MgO	17.18	0.83
Al <sub>2</sub> O <sub>3</sub>	60.03	1.45
Cr <sub>2</sub> O <sub>3</sub>	1.22	1.01
Sum Fe	20.11	1.61
FeO	15.12	1.37
Fe <sub>2</sub> O <sub>3</sub>	5.61	0.64
TiO <sub>2</sub>	0.41	0.10
Total	99.99	0.93

TABLE IV

COMPARISON OF EXSOLVED SPINELS AND HOST  
CLINOPYROXENE (FIGURES 29, 30)  
AND AVERAGE SPINEL AND CLINOPYROXENE  
FROM NODULE 1

	SPINEL			CPX	
	Exsol.	Aver.		Host	Aver.
Wt%			Wt%		
MgO	14.61	16.16	Na <sub>2</sub> O	1.09	1.07
Al <sub>2</sub> O <sub>3</sub>	51.80	59.04	MgO	13.68	12.85
TiO <sub>2</sub>	1.02	0.48	Al <sub>2</sub> O <sub>3</sub>	6.80	8.21
Cr <sub>2</sub> O <sub>3</sub>	6.06	0.44	SiO <sub>2</sub>	48.59	47.22
sum Fe	26.67	22.34	TiO <sub>2</sub>	1.47	1.74
FeO	18.67	16.55	CaO	19.88	20.41
Fe <sub>2</sub> O <sub>3</sub>	8.88	6.49	FeO	6.96	7.20
Total	101.04	99.72	Total	98.47	100.71

## BIBLIOGRAPHY

- Adams, G.E. and Bishop, F.C., 1982, Experimental investigation of Ca-Mg exchange between olivine, orthopyroxene and clinopyroxene: potential for geobarometry: *Earth and Planet. Sci. Lett.*, v.57, p. 241-250.
- Arculus, R.J., 1974, Melting behavior of two basanites in the range 10-35 kbar and the effect of  $TiO_2$  on the olivine-diopside reactions at high pressures: *Carnegie Inst. Wash. Yearbook* 74, p. 512-515.
- Arculus, R.J. and Delano, J.W., 1981, Intrinsic oxygen fugacity measurements: techniques and results for spinels from upper mantle peridotites and megacryst assemblages: *Geochem. and Cosmochim. Acta*, v.45, p. 899-913.
- Arculus, R.J., Dawson, J.B., Mitchell, R.H., Gust, D.A. and Holmes, R.D., 1984, Oxidation states of the upper mantle recorded by megacryst ilmenite in kimberlite and type A and B spinel lherzolites: *Contrib. Mineral. Petrol.*, v.85, p. 85-94.
- Augustithis, S.S., 1979, Atlas of the Textural Patterns of Basic and Ultrabasic Rocks and their Genetic Significance: Walter de Gruyter; Berlin, New York.
- Auricchio, C., Brotzy, P., Morbidelli, L., Piccirillo, E.M. and Traversa, G., 1983, Basanite to peralkaline phoholite suite: quantitative crystal fractionation model (Nyambenia Range, East Kenya Plateau): *Neus. Jahrbuch Miner. Abh.*, v.148, p. 113-140
- Bergman, S.C. and Dubessey, J., 1984,  $CO_2$ -CO fluid inclusions in a composite peridotite<sup>2</sup> xenolith: implications for upper mantle oxygen fugacity: *Contrib. Mineral. Petrol.*, v. 85, p. 1-13.
- Boyd, F.R. 1973, A pyroxene geotherm: *Geochim. et Cosmochim. Acta*, v. 37, p. 2533-2546.
- Bultitude, R.J. and Green, D.H., 1971, Experimental studies of crystal-liquid phase relationships at high pressures in olivine nephelinite and basanite compositions: *Jl. Petrol.*, v.12, p. 121-147.
- Buntin, T.J., 1983, An Oxygen, Iron, Carbon Geochemical Study of Selected Merensky Reef Potholes and their Possible Role in Merensky Reef Petrogenesis: unpublished M.A. Thesis, Temple University, Phila. Pa.

- Clark, S.P., Jr. and Ringwood, A.E., 1964, Density distributions and constitution of the mantle: Rev. Geophys. Space Phys., v.2, p. 35-68.
- Conlan, J., 1983, Ophiolites: unpublished undergraduate review paper, Temple University, Phila. Pa.
- Darken, L.S. and Gurry, R.W., 1945, The system iron-oxygen: I, the wustite field and related equilibria: Jl. Am. Chem. Soc., v. 67, p. 1398-1412.
- Davis, G.L. and Grew, E.S., 1977, Age of a zircon from a crustal xenolith, Kilbourne Hole, New Mexico: Carnegie Inst. Wash. Yearbook 77, p. 897-898.
- Deines, P., Nafziger, R.H., Ulmer, G.C. and Woermann, E., 1974, Temperature-oxygen fugacity tables for selected gas mixtures in the system C-H-O at one atmosphere total pressure: Bull. Earth and Min. Sci. Exp. Sta., Penn. State Univ.
- Dickinson, W.R. and Snyder, W.S., 1979, Geometry of subducted slabs related to the San Andreas transform: Jl. Geol., v. 87, p. 609-627.
- Duba, A., Piwinski, A.J., Heard, H.C. and Schock, R.N., 1974, The electrical conductivity of fosterite, enstatite and albite: in, The Physics and Chemistry of Minerals and Rocks; Wiley, New York.
- Eaton, G.P., 1979, A plate-tectonic model for late Cenozoic crustal spreading in the western United states: in, Riecker, R.E., ed., Rio Grande Rift: Tectonic and Magmatism; A.G.U., Washington D.C.
- Eugster, H.P. and Wones, D.R., 1962, Stability relations of the ferruginous biotite, annite: Jl. Petrol., v. 3, p. 82-125.
- Finger, L.W. and Hadidicos, C.G., 1971, Aspects of computer automation of an electron microprobe: Carnegie Inst. Year Book 70, p. 269-275.
- Freer, R. 1981, Diffusion in silicate minerals and glass: a data digest and guide to the literature: Contrib. Mineral. Petrol., v. 76, p. 414-454.
- Friel, J.J. and Ulmer, G.C., 1974, Oxygen fugacity geothermometry of the Oka carbonitite: Am. Min. v. 59, p. 314-318.

- Shaw, H.R., 1980, The fracture mechanisms of magma transport to the surface: in, Hargraves, R.B., ed., Physics of Magmatic Processes: Princeton Univ. Press, Princeton, p. 201-265.
- Simmons, G. and Richter, D., 1974, Microcracks in rocks: in, Strens, R.G.J., ed., The Physics and Chemistry of Rocks and Minerals: Wiley-Interscience, New York, p. 105-137.
- Spera, F.J., 1980, Aspects of magma transport: in, Hargraves, R.B., ed., Physics of Magmatic Processes: Princeton Univ. Press, Princeton, p. 265-323.
- Spera, F.J. and Bergman, S.C., 1980, Carbon dioxide in igneous petrogenesis I: aspects of the dissolution of CO<sub>2</sub> in silicate liquids: Contrib. Mineral. Petrol., v. 74, p. 55-66.
- Spry, A., 1969, Metamorphic Textures: Pergamon Press, London.
- Streckheisen, A., 1975, To each plutonic rock its proper name: Earth Sci. Rev., v. 12, p. 1-33.
- Thrush, P.W., ed., 1968, A Dictionary of Mining, Mineral and related Terms: U.S. Dept of the Interior, Washington, D.C.
- Ulmer, G.C., 1970, Chromite Spinels: in; Alper, A.M., ed., High Temperature Oxides: Part I, Magnesia, Lime and Chrome Refractories: Academic Press, New York.
- Ulmer, G.C., Rosenhauer, M., Woermann, E., Ginder, J., Drory-Wolff, A. and Wasilewski, P., 1976, Applicability of electro-chemical oxygen fugacity measurements to geothermometry. Am. Min., v. 61, p. 653-660.
- Williams, H., Turner, F.J. and Gilbert, C.H., 1982, Petrography An Introduction to the Study of Rocks in Thin Section, 2nd ed.: W.H. Freeman and Co., San Francisco.
- Wilshire, H.G. and Jackson, E.D., 1974, Problems in determining mantle geotherms from pyroxene compositions of ultramafic rocks: Jl. Geol., v. 83, p. 313-329.
- Wilshire, H.G. and Shervais, J.W., 1975, Al-augite and Cr-diopside ultramafic xenoliths in basaltic rocks from western United States: Phys. and Chem. of the Earth, v. 9, p. 257-272.

Wilson, E.D. Moore, R.T. and Pierce, H.W., 1959, Geologic Map of Gila County Arizona: Arizona Bureau of Mines, Univ. of Arizona.

Wohletz, K.H., Holloway, J.R., Cross, C. and Wilshire, H.G., 1977, Basalt Nodule Guide: Second Int'l Kimberlite Conference.

Yoder, H.S., 1976, Generation of Basaltic Magma: Natl. Acad. Sci., Washington, D.C.

APPENDIX I

GEO THERMOMETRY AND GEOBAROMETRY

NODULE n		Mercier (1976) Single Pyroxene Geothermometer & Geobarometer				Herzberg & Chapman (1976) CPX-OL-SP 12-kb calculations	
		x(T°C)	s	x(Pkb)s		x(T°C)	s
1	4	917.83	52.15	7.00	1.79	956.01	18.73
2	6	954.49	27.83	8.06	1.04	926.43	15.77
3	4	998.87	9.96	10.90	0.49	995.19	18.78
6	8	962.11	52.10	9.30	2.58	963.76	30.72

Adams and Bishop (1981) Results for San Carlos

Minerals (not specified, Group I or II)

910-1020°C      8-18 kb

- Frey, F.A. and Prinz, M., 1978, Ultramafic inclusions from San Carlos, Arizona: petrologic and geochemical data bearing on their petrogenesis: *Earth and Planet. Sci. Lett.*, v. 38, p. 129-176.
- Gary, H., McAfee, R. and Wolf, C., eds., 1972, *Glossary of Geology*: American Geological Institute, Washington, D.C.
- Greskovich, C.D., 1968, Precipitation and diffusion phenomena in the system  $MgO-Al_2O_3-Cr_2O_3$ : unpublished PhD thesis, Penn. State Univ.
- Griffin, W.L., Wass, S.Y. and Hollis, J.D., 1984, Ultramafic xenoliths from Bullenmerri and Gnotuk Maars, Victoria, Australia: Petrology of a subcontinental crust-mantle transition: *Jl. Petrol.*, v. 25, p. 53-87.
- Harris, P.G., Hutchinson, R. and Paul, D.K., 1972, Plutonic xenoliths and their relationship to the upper mantle: *Phil. Trans. R. Soc. Lon., Ser. A.*, v. 271, p. 313-323.
- Herzberg, C.T. and Chapman, N.A., 1976, Clinopyroxene geothermometry of spinel lherzolites: *Am. Min.* v. 61, p. 599-603.
- Irving, A.J., 1980, Petrology and geochemistry of composite ultramafic xenoliths in alkalic basalts and implications for magmatic processes within the mantle: *Am. Jl. Sci.*, v. 280-A, p. 389-426.
- Irving, A.J., 1976, On the validity of paleogeotherms determined from xenolith suites in basalts and kimberlites: *Am. Mineral.*, v. 61, p. 638-643.
- Jones, B., 1983, Peridot, Arizona's green gemstone: the major world supply is controlled by the San Carlos Apache: *Rock and Gem*, v. 13, p. 52-55.
- Kohlstedt, D.L., Goetze, C. and Durham, W.B., 1974, Experimental deformation of single crystal olivine with application to flow in the mantle: in, *Physics and Chemistry of Minerals and Rocks*, Strens, R.G.J., ed., Wiley-Interscience, p. 35-49.
- Koseluk, R.A., Elliot, W.C. and Ulmer, G.C., 1979, Gas inclusions and  $fO_2$  data from San Carlos, Arizona: *EOS, Trans. A.G.U.*, v. 60, p. 419.
- Kushiro, I., Syono, Y. and Akimoto, S., 1968, Melting of a peridotite at high pressures and high water pressure: *J. Geophys. Res.*, v. 73, p. 6023-6029.

- Kutolin, V.A. and Frova, V.M., 1970, Petrology of ultrabasic inclusions from basalts of Minosa and Transbaikalian regions (Siberia, USSR): *Contrib. Mineral. Petrol.*, v. 29, p. 163-179.
- Lausen, C., 1927 The occurrence of olivine bombs near Globe, Arizona: *Am. Jl. Sci.*, v. 14, p. 293-314.
- Lindsley, D.H., 1983, Pyroxene thermometry: *Am. Min.*, v. 63, p. 477-493
- Mercier, J-C., 1976, Single-pyroxene geothermometry and geobarometry: *Am. Min.*, v. 61, p. 603-616.
- Mercier, J-C. and Carter, N.L., 1975, Pyroxene geotherms: *J.G.R.*, v. 80, p. 3349-3362.
- Mercier, J-C., 1975, Textures and fabrics of upper-mantle peridotites as illustrated by xenoliths from basalts: *Jl. of Petrol.*, v. 16, p. 454-487.
- Misener, D.J., 1974, Cationic diffusion in olivine to 1400°C and 35 Kbar: in, Hoffman, A., Giletti, B.J. and Yund, R., eds., *Geochemical Transport and Kinetics*: Carnegie Inst. Wash. pub. 634.
- Mysen, B.O. and Boettcher, A.L., 1975, Melting of a hydrous mantle: I, phase relations of a natural peridotite at high pressures and temperatures with controlled activities of water, carbon dioxide and hydrogen: *J. Petrol.*, v. 16, p. 255-258
- Nicholas, A. and Jackson, M., 1982, High temperature dikes in peridotites: origin by hydraulic fracturing: *Jl. Petrol.*, v. 23, p. 568-582.
- Oberheuser, G., Kathrein, H., Demortier, G., Gonska, H. and Freund, F., 1983, Carbon in olivine single crystals analyzed by the  $^{12}\text{C}(d,p)^{13}\text{C}$  method and by photoelectron spectroscopy: *Geochim. Cosmochim. Acta*, v. 47, p. 1117-1129.
- Phillips, W.R. and Griffen, D.T., 1981, *Optical Mineralogy, the Non-Opaque Minerals*: W.H. Freeman and Co., San Francisco.
- Robie R.A., Hemingway, B.S. and Fisher, J.R., 1979, Thermodynamic properties of minerals and related substances at 298.15 K and 1 bar ( $10^5$  Pascals) pressures and at higher temperatures: *Geol. Soc. Am. Bull.* 1452, U.S.G.P.O., Washington, D.C.
- Roedder, E., 1965, Liquid  $\text{CO}_2$  inclusions in olivine-bearing

nodules and phenocrysts from basalts: *Am. Min.*, v. 50, p. 1746-1782.

Roedder, E., 1984, "Fluid Inclusions in Terrestrial and Lunar Geological Settings": in press

Roiter, B.D., Phase equilibria in the spinel region of the system  $\text{FeO-Fe}_2\text{O}_3\text{-Al}_2\text{O}_3$ : *Jl. Am. Ceram. Soc.*, v. 47, p. 509-511.

Sato, M., 1965, Electrochemical geothermometry: A possible new method of geothermometry with electroconductive minerals: *Eco. Geo.*, v. 60, p. 812-818.

Sato, M., 1971, Electrochemical measurement and control of oxygen fugacity and other gaseous fugacities with solid electrolyte sensors: in, Ulmer, G.C., ed., *Research Techniques for High Pressure and High Temperature*: Springer-Verlag, New York.

Sato, M., 1972, Intrinsic oxygen fugacities of iron-bearing oxide and silicate minerals under low total pressure: *Geol. Soc. Am. Mem.* 135, p. 289-307.

Sato, M. and Valenza, M., 1980, Oxygen fugacities of the layered series of the Skaergaard intrusion, East Greenland: *Am. Jl. Sci.*, v. 280-A, p. 134-158.

Scarfe, C.M., Takahashi, E. and Yoder, H.S., 1980, Rates of dissolution of upper mantle minerals in an alkali-olivine basalt melt at high pressures: *Carnegie Inst. Wash. Yearbook* 80, p. 290-295.

Schaefer, M.W., 1983, Crystal Chemistry of Ferric-Rich Fayalites: unpublished PhD dissertation, Mass. Inst. Technol., Cambridge, Mass.

Seager, W.R. and Morgan, P., 1979, Rio Grande Rift in southern New Mexico, West Texas and northern Chihuahua: in, Reiker, R., ed. *Rio Grande Rift: Tectonics and Magmatism*: A.G.U., Washington, D.C.

Seager, W.R., Shafiqullah, M., Howley, J.W. and Marum, R.F., 1984, New K-Ar dates from basalts and the evolution of the southern Rio Grande Rift: *Geol. Soc. Am. Bull.*, 95, p. 87-99.

Shearer, C. and Reiter, M., 1980, Terrestrial heat flow in Arizona: *J.G.R.*, v. 86, p. 6249-6268.

APPENDIX II: COMPUTER PROGRAMS  
IN BASIC FOR CALCULATING  
GEO THERMOMETRY AND GEOBAROMETRY  
i. Mercier (1976)  
ii. Herzberg and Chapman (1976)

Written for use on Apple IIe

NOTE: The equation used for geobarometric calculations in the first program (line 430) differs from the original Mercier (1976) equation in that a negative sign appears in the numerator in place of the original positive sign. The change of sign was made so that the Mercier equation would produce reasonable and relatively consistent results.

JPR#0  
JLIST

```
90 REM MERCIER CPX GEOTHERM, GEOBARDM, SPINEL FACIES: ARRAY METHOD
110 D# = CHR# (4)
130 PRINT "MERCIER SINGLE PYROXEN          E GEOTHERMOMETER, GEOBAROME
      T          ER, SPINEL FACIES, CPX: AM M          IN 61, PP 603-6
16": PRINT D#;"PR#1"
150 PRINT "MERCIER SINGLE PYROXENE GEOTHERMOMETER, GEOBAROMETER, SPINEL
      FACIES, CPX: AM MIN 61, PP 603-616": PRINT D#;"PR#0"
170 FOR I = 1 TO 5
190 REM ENTER SAMPLE ID
210 INPUT "SAMPLE ID= ";PYX#(I): PRINT D#;"PR#1": PRINT "SAMPLE ID= ";PY
      X#(I): PRINT D#;"PR#0"
230 REM ENTER CATIONS PER 6 OXYGEN
250 GOSUB 530
270 REM CALCULATE AL SITE DISTRIBUTION
290 GOSUB 750
310 REM CALCULATE FE CHARGE DISTRIBUTION
330 GOSUB 870
350 REM CALCULATE PARAMETERS
370 GOSUB 950
390 TDEGC(I) = ((( - 7537.5 * Y(I)) + 61152) / D(I)) - 273.15
410 REM CALCULATE P KB
430 P(I) = ((419.76 * Y(I)) - (706 * X(I)) + 493.49) / D(I)
450 PRINT PYX#(I); TAB( 16)( INT (100 * TDEGC(I))) / 100;"C"; TAB( 32)( INT
      (100 * P(I))) / 100;"KB": PRINT D#;"PR#1": PRINT PYX#(I); TAB( 16)( INT
      (100 * TDEGC(I))) / 100;"C"; TAB( 32)( INT (100 * P(I))) / 100;"KB"
470 PRINT D#;"PR#0"
490 NEXT I
510 GOTO 1150
530 REM LIST CATIONS
550 INPUT "NA= ";NA(I): PRINT D#;"PR#1": PRINT "NA= ";NA(I): PRINT D#;"P
      R#0"
570 INPUT "MG= ";MG(I): PRINT D#;"PR#1": PRINT "MG= ";MG(I): PRINT D#;"P
      R#0"
590 INPUT "AL= ";AL(I): PRINT D#;"PR#1": PRINT "AL= ";AL(I): PRINT D#;"P
      R#0"
610 INPUT "SI= ";SI(I): PRINT D#;"PR#1": PRINT "SI= ";SI(I): PRINT D#;"P
      R#0"
630 INPUT "CA= ";CA(I): PRINT D#;"PR#1": PRINT "CA= ";CA(I): PRINT D#;"P
      R#0"
650 INPUT "TI= ";TI(I): PRINT D#;"PR#1": PRINT "TI= ";TI(I): PRINT D#;"P
      R#0"
670 INPUT "CR= ";CR(I): PRINT D#;"PR#1": PRINT "CR= ";CR(I): PRINT D#;"P
      R#0"
690 INPUT "MN= ";MN(I): PRINT D#;"PR#1": PRINT "MN= ";MN(I): PRINT D#;"P
      R#0"
710 INPUT "FE= ";FE(I): PRINT D#;"PR#1": PRINT "FE= ";FE(I): PRINT D#;"P
      R#0"
730 RETURN
750 REM AL SITES
770 REM AN=ALIV
790 AN(I) = 2 - SI(I)
810 REM AN=ALVI
830 AN(I) = AL(I) - AN(I)
850 RETURN
870 REM FE CHARGE DIST
890 F3(I) = AN(I) + NA(I) - CR(I) - AN(I) - (2 * TI(I))
910 F2(I) = FE(I) - F3(I)
930 RETURN
950 REM PARAMETERS
970 A(I) = (AL(I) + CR(I) - NA(I)) / 2
990 W(I) = CA(I) / (CA(I) + MG(I) + MN(I) + F2(I))
1010 KS(I) = 0.9 + (1.29 * (CR(I) / A(I)) ^ 3)
1030 KA(I) = KS(I) * (A(I) * (1 - A(I)))
1050 X(I) = LOG (KA(I))
1070 KW(I) = (1 - (2 * W(I))) / (0.65 + (0.7 * W(I)))
1090 Y(I) = LOG (KW(I))
1110 D(I) = X(I) * Y(I) - (11.098 * Y(I)) + (2.26 * X(I)) + 32.765
1130 RETURN
9999 END
```

JPR#0  
LIS1

```
10 REM HERZBERG AND CHAPMAN CPX GEOTHERMOMETER
11 D* = CHR$(4)
15 PRINT "HERZBERG AND CHAPMAN C PX GEOTHERMOMETER, AM. MIN.
      V61 PP 626-638"; PRINT D*;"PR#1"
16 PRINT "HERZBERG AND CHAPMAN CPX GEOTHERMOMETER, AM MIN V61 PP 626-638
      ": PRINT D*;"PR#0"
20 FOR I = 1 TO 5
30 REM ENTER SAMPLE ID
40 INPUT "ID=(PX),(OL),(SP)"; ID*(I): PRINT D*;"PR#1": PRINT "ID=(PX),(OL
      ).(SP)"; ID*(I): PRINT D*;"PR#0"
50 REM ENTER CATIONS FOR CPX,OL,SP
60 GOSUB 300
65 PRINT "ID","T-12KB","T-16KB": PRINT D*;"PR#1": PRINT "ID"; TAB( 22);"
      T-12KB"; TAB( 32);"T-16KB": PRINT D*;"PR#0"
70 REM CALCULATE AL SITE DISTRIBUTION
80 GOSUB 400
90 REM CALCULATE FE CHARGE DISTRIBUTION
100 GOSUB 500
110 REM CALCULATE ACTIVITIES
120 GOSUB 600
130 REM CALCULATE LN K
140 LNK(I) = LOG ((A1(I) * A3(I)) / (A2(I) * A4(I)))
150 REM CALC T AT 12 KB=TT
160 TT(I) = - 8340 / (LNK(I) - 4.06)
165 TT(I) = (( INT (100 * TT(I))) / 100) - 273.15
170 REM CALC T AT 16KB=TS
175 TS(I) = - 9231 / (LNK(I) - 4.46)
180 TS(I) = (( INT (100 * TS(I))) / 100) - 273.15
190 PRINT ID*(I); TAB( 16);TT(I);"C"; TAB( 32);TS(I);"C": PRINT D*;"PR#1
      ": PRINT ID*(I); TAB( 16);TT(I);"C"; TAB( 32);TS(I);"C": PRINT D*;"P
      R#0"
200 NEXT I
210 GOTO 900
300 REM CPX CATIONS/OXYGEN
310 INPUT "NA= ";NA(I): PRINT D*;"PR#1": PRINT "NA= ";NA(I): PRINT D*;"P
      R#0"
315 INPUT "MG= ";MG(I): PRINT D*;"PR#1": PRINT "MG= ";MG(I): PRINT D*;"P
      R#0"
320 INPUT "AL= ";AL(I): PRINT D*;"PR#1": PRINT "AL= ";AL(I): PRINT D*;"P
      R#0"
325 INPUT "SI= ";SI(I): PRINT D*;"PR#1": PRINT "SI= ";SI(I): PRINT D*;"P
      R#0"
330 INPUT "CA= ";CA(I): PRINT D*;"PR#1": PRINT "CA= ";CA(I): PRINT D*;"P
      R#0"
335 INPUT "TI= ";TI(I): PRINT D*;"PR#1": PRINT "TI= ";TI(I): PRINT D*;"P
      R#0"
340 INPUT "CR= ";CR(I): PRINT D*;"PR#1": PRINT "CR= ";CR(I): PRINT D*;"P
      R#0"
345 INPUT "MN= ";MN(I): PRINT D*;"PR#1": PRINT "MN= ";MN(I): PRINT D*;"P
      R#0"
350 INPUT "FE= ";FE(I): PRINT D*;"PR#1": PRINT "FE= ";FE(I): PRINT D*;"P
      R#0"
360 INPUT "OL MG= ";OMG(I): PRINT D*;"PR#1": PRINT "OL MG= ";OMG(I): PRINT
      D*;"PR#0"
370 INPUT "SP MG= ";SMG(I): PRINT D*;"PR#1": PRINT "SP MG= ";SMG(I): PRINT
      D*;"PR#0"
380 RETURN
400 REM ALUMINUM SITE DISTRIBUTION
410 REM ALIV=AM
420 AM(I) = 2 - SI(I)
430 REM ALVI=AN
440 AN(I) = AL(I) - AM(I)
450 RETURN
500 REM FE CHARGES
510 REM F3=FE3+, F2=FE2+
520 F3(I) = AN(I) + NA(I) - CR(I) - AN(I) - (2 * TI(I))
530 F2(I) = FE(I) - F3(I)
540 RETURN
600 REM ACTIVITY CALCULATION
610 A1(I) = AN(I) ^ 2
620 A2(I) = (CA(I) - AN(I)) ^ 2
630 A3(I) = (OMG(I) / 2) ^ 2
640 A4(I) = (SMG(I)) ^ 2
650 RETURN
900 END
```

### APPENDIX III

#### Diffusion: Olivine and Spinel

Calculations for the interdiffusion of Mg and Fe in olivine have been made, data used is from Buening and Buseck (ref. 13) in Freer (1981). Temperature dependence of D (diffusion rate) is given by the equation:

$$D = D_0 \exp(-Q/RT)$$

where  $D_0$  ( $m^2 s^{-1}$ ) is the pre-exponential factor (= D at  $1/T=0$ ), Q is the activation energy ( $J mol^{-1}$ ), R is the gas constant ( $8.314 J ^\circ K^{-1} mol^{-1}$ ) and T the temperature ( $^\circ K$ ). Diffusion times can be calculated by the formula:  $x^2 = Dt$ , where x = distance and t = time. All of the above parameters and the equation are universal, that is not limited to olivine.

	$T=1273^\circ K$	$T=1373^\circ K$	$T=1473^\circ K$
	$D=10^{-15.40}$	$D=10^{-15.04}$	$D=10^{-14.39}$
(x equals distance in cm, t equals time in years.)			
x=0.1	$t=10^{1.9}$	$t=10^{1.5}$	$t=10^{0.9}$
x=1.0	$t=10^{3.9}$	$t=10^{3.5}$	$t=10^{2.9}$
x=10	$t=10^{5.9}$	$t=10^{5.5}$	$t=10^{4.9}$

These calculations are for Po 92-97 at one atmosphere. Meisner (1974) states that diffusion rates for olivine decrease with increased pressure and increase with increasing Fe content, the offsetting factors are taken as equal here.

Diffusion rates for  $\text{Cr}_2\text{O}_3$  in spinel have been estimated by extrapolating the high-temperature (1600-1300°C) data of Greskovich (1968) to 1100°C. Resulting from this extrapolation is an interdiffusion coefficient for Cr/Mg in spinel of  $10^{-16.81}$ . This D value is almost two orders of magnitude slower than the interdiffusion coefficient ( $10^{-15.04}$ ) for Fe/Mg in olivine at this temperature. This estimated interdiffusion coefficient of Cr/Mg in spinel relative to Fe/Mg in olivine supports the suggestion presented in this thesis that spinel phase chemistry heterogeneity and olivine homogeneity in the same nodule could be a function of relative diffusion rates in the two phases.

## APPENDIX IV

### IOP PROBLEMS

PROBLEM I: Iron in Pt cell cap. Incorporated during tink-welding process used to make Pt foil into cylindrical cap.

SYMPTOMS: Unchanging 800 mv reading on EMF meter during IOP analysis. Iron contamination visible under highest power on binocular microscope.

SOLUTION: HCl treatment of Pt cap. Heat cap in bunsen burner flame until red hot, then plunge into beaker of HCl. Repeat 5-10 times or until yellow Fe-Cl compounds stop coming from Pt.

PROBLEM II: Ag-Hydrides on Ag-Pd sample bucket, formed during reduction of Ag-oxides (resulting from bucket making process) in H<sub>2</sub> torch flame.

SYMPTOMS: 800 mv signal on EMF meter during IOF analysis. Slight blackening or dulling of sample bucket visible after experiment.

SOLUTION: Reduce Ag-oxides in Bunsen burner flame (less reducing than H<sub>2</sub> flame).

PROBLEM III: Sample bucket collapse when run in air during blank correction analysis.

SYMPTOMS: EMF readings fluctuate considerably during IOF analysis, eventually going off-scale, indicating a broken connection.

SOLUTION: Reinforce sample bucket with an extra loop of wire.

PROBLEM IV: Copper contamination of  $\text{Ag}_{60}\text{Pd}_{40}$  wire at manufacturer's during drawing process.

SYMPTOMS: 800 mv signal during IOF analyses that gradually deteriorates to about 100 mv over 2-3 hours at temperature. Wire is blackened when removed from cell after experiment.

SOLUTION: Complaints to manufacturer. Specification of <50 ppm Cu for wire order. Tighter quality control at manufacturer's.

PROBLEM V: Organic lubricant (stearate compound) contamination of  $\text{Ag}_{60}\text{Pd}_{40}$  wire at manufacturer's during drawing process.

SYMPTOMS: Strong reducing signal on sample cell EMF meter and black smoke emanating from sample cell during analysis. Wire and Vycor is blackened or yellowed when removed from cell after experiment.

SOLUTION: Wipe down each length of wire with warm water and a bit of soap before each analysis. Inspect wire under binocular microscope to ensure that it is contamination free.

APPENDIX V: COMPUTER PROGRAM  
IN BASIC FOR CALCULATING  
FLUID INCLUSION/PARTIAL PRESSURE  
RELATIONSHIPS

Written for use on Apple IIe

IPRHO  
JLIST

```
10 REM THIS PROGRAM CALCULATES PERCENT PARTIAL PRESSURE
20 REM TOTAL PRESSURE IS NORMALIZED TO ONE ATMOSPHERE
30 REM PERCENT PARTIAL PRESSURE EQUALS MOLE FRACTION
100 REM PROGRAM TO CALCULATE FLUID INCLUSION/PARTIAL PRESSURE OF INCLUS
    ION PHASE RELATIONSHIPS
200 REM ALL DATA IN CM, G, ATM
300 D# = CHR# (4)
400 PRINT "PROGRAM TO CALCULATE"
500 PRINT "FLUID INCLUSION PARAMETERS"
600 PRINT " "
700 PRINT "ENTER DATA IN CM, G"
800 PRINT " "
900 INPUT "SAMPLE COMPOSITION IS: ";SC#
1000 INPUT "FLUID COMPOSITION IS: ";FC#
1100 INPUT "DIAMETER OF INCLUSION (CM)= ";DI
1200 INPUT "GMM OF INCLUSION SPECIES= ";GF
1300 INPUT "DENSITY OF FLUID (G/CC)= ";RF
1400 REM CALCULATE VOL OF INCLUSION
1500 VI = (4.1867) * ((DI / 2) ^ 3)
1600 REM CALCULATE MOLES OF FLUID IN INCLUSION
1700 MF = RF * VI * (1 / GF)
1800 REM ENTER SOLID SAMPLE PARAMETERS
1900 INPUT "GMM OF SAMPLE SPECIES= ";GS
2000 INPUT "DENSITY OF SAMPLE (G/CC)= ";RS
2100 INPUT "MASS OF SAMPLE (G)= ";MS
2200 INPUT "AV. DIAM. OF SAMPLE GRAIN (CM)= ";DS
2300 REM CALCULATE SOLID SAMPLE PARAMETERS
2400 VS = (4 / 3) * 3.14 * ((DS / 2) ^ 3)
2500 NG = (1 / (RS * VS)) * MS
2600 NB = INT (1 * NG) / 1
2700 NX = 10000 / NG
2800 NX = INT (NX * 100) / 100
2900 REM PARTIAL PRESSURE CALCULATIONS
3000 INPUT "VOLUME OF CELL FREE SPACE (CC)= ";VC
3100 REM CALCULATE MOLES OF GAS IN FREE SPACE
3200 NG = VC * (1 / 22400)
3300 REM CALCULATE TOTAL PRESSURE IN FREE SPACE (PT)
3400 REM IDEAL GAS APPROX: PV=NRT
3500 REM R=82.1, N=MG
3600 R = 82.1
3700 PRINT D#;"PR#1": PRINT "FLUID INCL/PART. PRESS CALCULATIONS"
3800 PRINT "SAMPLE COMPOSITION IS ";SC#
3900 PRINT "FLUID COMPOSITION IS ";FC#
4000 PRINT "AV GRAIN DIAMETER IS ";DS
4100 PRINT "NUMBER OF GRAINS/SAMPLE= "NG
4200 PRINT "FOR 10^4 INCL THERE WOULD BE ";NX;" INCL/GRAIN"
4300 PRINT " "
4320 PRINT "CALCULATION OF % PARTIAL PRESSURE (P.TOT.=1)": PRINT D#;"PR#
    0"
4400 PRINT " "
4500 REM NUMBER OF TEMP POINTS TO BE CONSIDERED
4600 INPUT "NUMBER OF TEMPS= ";N
4700 FOR I = 1 TO N
4800 INPUT "TEMP= ";T(I)
4900 PRINT D#;"PR#1"
5000 PRINT "FOR T= ";T(I)
5100 PRINT "INCL DIAM(CM)"; TAB( 15);"LOG #INCL": TAB( 20);"LOG %PART.PR
    ESS. (ATM)": PRINT D#;"PR#0"
5200 REM ENTER NUMBER OF INCL POPULATIONS TO BE CONSIDERED
5300 INPUT "NUMBER OF INCLUSION POPULATIONS= ";M
5400 FOR J = 1 TO M
5500 INPUT "NUMBER OF INCLUSIONS= ";NI(J)
5600 NI(J) = ( LOG (NI(J))) / 2.3025809
5700 NI(J) = ( INT (NI(J)) * 10) / 10
6000 REM CALCULATE PARTIAL PRESSURE (PP)
6150 PP(J) = ((10 ^ NI(J)) * MF) / (NG + (MF * (10 ^ NI(J))))
6200 PP(J) = ( LOG (PP(J))) / 2.3025809
6300 PP(J) = INT ((PP(J)) * 100) / 100
6400 PRINT DI; TAB( 15);NI(J); TAB( 25);PP(J)
6500 PRINT D#;"PR#1": PRINT " "
6600 PRINT DI; TAB( 23);NI(J); TAB( 29);PP(J)
6700 PRINT " "; PRINT D#;"PR#0"
6800 NEXT J
6900 NEXT I
9999 END
```